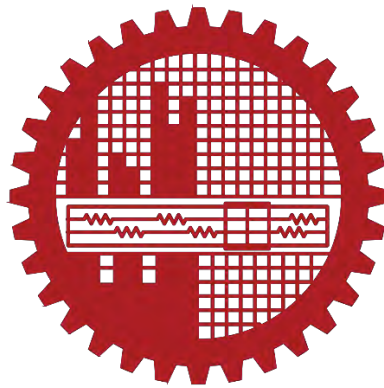


**Effect of Micro Groove on Condensation Behavior of Vertical
Copper Plate**

by

Md. Omarsany Bappy

MASTER OF SCIENCE IN MECHANICAL ENGINEERING



Department of Mechanical Engineering

BANGLADESH UNIVERSITY OF ENGINEERING AND TECHNOLOGY

November 2021

The thesis titled “Effect of Micro Groove on Condensation Behavior of Vertical Copper Plate” submitted by Md. Omarsany Bappy, St. Id: 1018102052, Session: October 2018, has been accepted as satisfactory in partial fulfillment of requirement for the degree of Master of Science in Mechanical Engineering on November 03, 2021.

BOARD OF EXAMINERS



Dr. A.K.M. Monjur Morshed

Professor
Department of Mechanical Engineering
BUET, Dhaka-1000

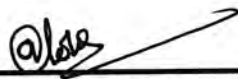
Chairman
(Supervisor)



Dr. Shaikh Reaz Ahmed

Professor and Head
Department of Mechanical Engineering
BUET, Dhaka-1000


Member
(Ex-officio)



Dr. Alope Kumar Mozumder

Professor
Department of Mechanical Engineering
BUET, Dhaka-1000


Member



Dr. Md. Zahurul Haq

Professor
Department of Mechanical Engineering
BUET, Dhaka-1000

Member



Dr. Md. Lutfor Rahman

Vice Chancellor
Bangladesh Army University of Science
and Technology (BAUST)

Member
(External)

CANDIDATE'S DECLARATION

It is hereby declared that this thesis or any part of this thesis has not been submitted elsewhere for any award or any degree or any diploma.

November 2021



Md. Omarsany Bappy

ACKNOWLEDGEMENTS

Firstly, I would like to thank the Almighty Allah for giving me the strength to complete this work.

I would like to express my sincere gratitude to my honorable supervisor, Dr. A. K. M. Monjur Morshed, for his continuous support, encouragement, motivation, and guidance throughout all phases of this M.Sc. engineering study. Without his persistent guidance and support, this dissertation would not be possible. It has been a great privilege and honor for me to work with him.

I would like to thank the members of my thesis evaluation committee, Dr. Shaikh Reaz Ahmed, Dr. Alope Kumar Mozumder, Dr. Md. Zahurul Haq and Dr. Md. Lutfor Rahman for their valuable comments and suggestions.

Finally, I would like to thank my family and friends for their encouragement and support, without which this dissertation and research would not have been possible.

“The secret of success is to do the common thing uncommonly well”

- John D. Rockefeller Jr.

ABSTRACT

Condensation is one of the most effective and efficient methods for transferring large amounts of heat, resulting in its widespread use in power generation, air-conditioning and refrigeration system, water desalination system, electronics thermal management, petroleum industry, chemical plant, and other applications. Condensation heat transfer is an efficient but complex phenomenon influenced by a number of factors including surface material properties, surface morphology, fluid properties, degree of sub-cooling, presence of impurities, and so on. Condensation heat transfer can be controlled or enhanced by controlling these factors and among those, surface modification is an easy and effective technique to enhance condensation heat transfer behavior. Condensation behavior on coated surfaces, hydrophilic surfaces, hydrophobic surfaces, and triangular grooved surfaces, etc. has already been widely studied, but the effect of rectangular, wedge and sinusoidal shaped micro groove on condensation behavior is yet to be investigated. Contact angle and droplet parameters such as droplet size, droplet frequency, droplet growth rate, droplet coalescence rate, droplet drainage rate, and others are affected by introducing various micro grooves on copper surfaces, and all these parameters, as well as heat transfer behavior, have been studied in this experimental study for both flat and micro-grooved vertical copper surfaces. In the case of micro-grooved copper surfaces, droplet density dropped, and droplet coalescence was reduced, indicating that smaller diameter droplets increased dropwise condensation. This smaller diameter droplets slide faster through the micro-grooved copper surfaces compared to the flat copper plate. As a result, the condensate drainage in modified copper plates is expedited, which improves the condensation behavior of the micro-grooved copper plates. Heat transfer behavior is also studied in terms of heat transfer coefficient. Heat transfer Co-efficient of wedge, sinusoidal and rectangular shaped micro-grooved surfaces are 15-18%, 15-50% and 20-60% higher than flat copper surface at same Sub-cooling temperature. This is due to the decrement of wettability and droplet density in case of modified copper surfaces. Plausible reason for this enhancement has been broadly discussed in this article.

TABLE OF CONTENTS

CANDIDATE’S DECLARATION	iii
ACKNOWLEDGEMENTS	iv
ABSTRACT	vi
LIST OF FIGURES	xi
LIST OF TABLES	xiii
NOMENCLATURE	xiv
CHAPTER 1: INTRODUCTION	1
1.1 Dropwise condensation	1
1.2 Filmwise condensation	2
1.3 Nucleation in vapors.....	3
1.3.1 Heterogeneous nucleation in vapors.....	3
1.4 Factors affecting condensation heat transfer	4
1.4.1 Vapor pressure	4
1.4.2 Heat flux	5
1.4.3 Surface Sub-cooling.....	5
1.4.4 Non-condensable gases.....	5
1.4.5 Vapor velocity	6
1.4.6 Droplet characteristics	7
1.4.7 Surface properties	9
1.4.8 Surface inclination	10
1.4.9 Working fluids	10
1.5 Applications of condensation heat transfer	11
1.5.1 Power generation	11
1.5.2 Desalination	11

1.5.3 Refrigeration and air-conditioning	12
1.5.4 Electronics thermal management.....	12
1.5.5 Petrochemical refining.....	12
1.5.6 Water harvesting.....	12
1.6 Motivation for the work	13
1.7 Objectives.....	14
1.8 Layout of the thesis	14
CHAPTER 2: LITERATURE REVIEW	15
2.1 Existing literature on condensation	15
2.2 Condensation heat transfer model	18
2.2.1 Nusselt's model.....	19
2.2.2 Background mechanism of dropwise condensation modeling	21
2.2.3 Correlation of Rose for dropwise condensation	22
2.2.4 First model.....	24
2.2.5 Second model.....	25
CHAPTER 3: EXPERIMENTAL PROCEDURE.....	26
3.1 Experimental setup design	26
3.1.1 Test loop	32
3.2 Data acquisition system.....	33
3.2.1 Steam flow rate	33
3.2.2 Cooling water flow rate	33
3.2.3 Condensate drainage rate.....	34
3.2.4 Temperature.....	34
3.2.5 Time.....	34
3.3 Experimental process	34
3.4 Data analysis	35

3.5 Uncertainty analysis	36
CHAPTER 4: EXPERIMENTAL RESULTS AND DISCUSSION	40
4.1 Study on surface wettability	40
4.2 Surface condensation morphology	41
4.2.1 Condensation morphology on flat copper plate.....	41
4.2.2 Condensation morphology on wedge shaped micro grooved copper plate.....	42
4.2.3 Condensation morphology on sinusoidal shaped micro grooved copper plate.....	44
4.2.4 Condensation morphology on rectangular shaped micro-grooved copper plate.....	46
4.3 Heat transfer analysis	48
4.3.1 Effect of Sub-cooling temperature on heat transfer Co-efficient for flat copper plate.....	48
4.3.2 Effect of Sub-cooling temperature on heat transfer Co-efficient for wedge shaped micro grooved copper plate	49
4.3.3 Effect of Sub-cooling temperature on heat transfer Co-efficient for sinusoidal shaped micro-grooved copper plate.....	50
4.3.4 Effect of Sub-cooling temperature on heat transfer Co-efficient for rectangular shaped micro-grooved copper plate.....	51
4.3.5 Comparative analysis of effect of Sub-cooling temperature on heat transfer Co-efficient of flat and modified copper surfaces	52
4.3.6 Effect of time on heat transfer Co-efficient for flat copper plate	53
4.3.7 Effect of time on heat transfer Co-efficient for wedge shaped micro-grooved copper plate.....	53
4.3.8 Effect of time on heat transfer Co-efficient for sinusoidal shaped micro-grooved copper plate.....	54
4.3.9 Effect of time on heat transfer Co-efficient for rectangular shaped micro-grooved copper plate.....	55

4.3.10 Comparative analysis of effect of time on heat transfer Co-efficient of flat and modified copper surfaces	56
CHAPTER 5: CONCLUSIONS	57
5.1 Conclusion.....	57
5.2 Future Recommendations.....	58
REFERENCES	59
APPENDIX.....	68
Appendix-1: Experimental data for flat copper plate.....	68
Appendix-2: Experimental data for wedge shaped micro-grooved copper plate...	76
Appendix-3: Experimental data for sinusoidal shaped micro-grooved copper plate	84
Appendix-4: Experimental data for rectangular shaped micro-grooved copper plate	92
Appendix 5: Sample calculation	100
Appendix 6: Sample calculation of uncertainty analysis	101

LIST OF FIGURES

Figure 1.1: Dropwise condensation	1
Figure 1.2: Filmwise condensation	2
Figure 1.3: An embryo liquid droplet formed at an idealized liquid- solid interface ..	4
Figure 1.4: Schematic of static and dynamic contact angles	8
Figure 1.5: Schematic showing wetting regimes over rough surface (a) Wenzel state (b) Partially wetting state (c) Cassie-Baxter or Suspended state.	8
Figure 3.1: Constructed experiment chamber	26
Figure 3.2: Flat copper plate	27
Figure 3.3: Rectangular shaped micro-grooved copper plate	28
Figure 3.4: Sinusoidal shaped micro-grooved copper plate.....	29
Figure 3.5: Wedge shaped micro-grooved copper plate	30
Figure 3.6: Constructed mini boiler	31
Figure 3.7: Submersible pump	32
Figure 3.8: Experimental setup for the condensation heat transfer experiment	32
Figure 3.9: Actual photo of experimental setup.....	35
Figure 4.1: Contact angle of droplets on flat and micro-grooved copper plate	40
Figure 4.2: Condensation morphology on flat copper plate (3x magnification).....	42
Figure 4.3: Condensation morphology on wedge shaped micro-grooved copper plate (3x magnification).....	43
Figure 4.4: Condensation morphology on sinusoidal shaped micro-grooved copper plate (3x magnification).....	45
Figure 4.5: Condensation morphology on rectangular micro-grooved copper plate (3x magnification)	47
Figure 4.6: Variation of heat transfer Co-efficient with temperature difference for flat copper plate	48
Figure 4.7: Variation of heat transfer Co-efficient with temperature difference for both flat and wedge shaped micro-grooved copper plate	49
Figure 4.8: Variation of heat transfer Co-efficient with temperature difference for both flat and sinusoidal shaped micro-grooved copper plate.....	50

Figure 4.9: Variation of heat transfer Co-efficient with temperature difference for both flat and rectangular shaped micro-grooved copper plate	51
Figure 4.10: Variation of heat transfer Co-efficient with temperature difference for both flat and modified copper surfaces	52
Figure 4.11: Variation of heat transfer Co-efficient with time for flat copper plate..	53
Figure 4.12: Variation of heat transfer Co-efficient with time for both flat and wedge shaped micro-grooved copper plate	53
Figure 4.13: Variation of heat transfer Co-efficient with time for both flat and sinusoidal shaped micro-grooved copper plate	54
Figure 4.14: Variation of heat transfer Co-efficient with time for both flat and rectangular shaped micro-grooved copper plate	55
Figure 4.15: Variation of heat transfer Co-efficient with time for both flat and modified copper surfaces	56

LIST OF TABLES

Table 1: Bias limit of measurands	37
Table 2: Uncertainty in estimated parameters	39
Table 3: Experimental data for flat copper plate.....	68
Table 4: Calculation of area and mass flow rate for flat copper plate	70
Table 5: Calculation of heat flux for flat copper plate.....	70
Table 6: Calculation of heat transfer Co-efficient for flat copper plate.....	73
Table 7: Experimental data for wedge shaped micro-grooved copper plate.....	76
Table 8: Calculation of area and mass flow rate for wedge shaped micro-grooved copper plate	78
Table 9: Calculation of heat flux for wedge shaped micro-grooved copper plate.....	78
Table 10: Calculation of heat transfer Co-efficient for wedge shaped micro-grooved copper plate	81
Table 11: Experimental data for sinusoidal shaped micro-grooved copper plate.....	84
Table 12: Calculation of area and mass flow rate for sinusoidal shaped micro- grooved copper plate	86
Table 13: Calculation of heat flux for sinusoidal shaped micro-grooved copper plate	86
Table 14: Calculation of heat transfer Co-efficient for sinusoidal shaped micro- grooved copper plate.....	89
Table 15: Experimental data for rectangular shaped micro-grooved copper plate	92
Table 16: Calculation of area and mass flow rate for rectangular shaped micro- grooved copper plate	94
Table 17: Calculation of heat flux for rectangular shaped micro-grooved copper plate	94
Table 18: Calculation of heat transfer Co-efficient for rectangular shaped micro- grooved copper plate.....	97

NOMENCLATURE

T_1	Upper copper plate temperature ($^{\circ}\text{C}$)
T_2	Cooling water outlet temperature ($^{\circ}\text{C}$)
T_3	Lower copper plate temperature ($^{\circ}\text{C}$)
T_4	Steam inlet temperature ($^{\circ}\text{C}$)
T_5	Cooling water inlet temperature ($^{\circ}\text{C}$)
T_{surf}	Average condensing surface temperature ($^{\circ}\text{C}$)
\dot{m}_c	Mass flow rate of cooling water (kg/sec)
C_p	Specific heat of cooling water at constant pressure (J/kg.K)
q	Heat flux on condensing surface during condensation (W/m^2)
A	Effective condensation area (m^2)
h_c	Heat transfer Co-efficient ($\text{W}/\text{m}^2.\text{K}$)
ΔT	Sub-cooling temperature ($^{\circ}\text{C}$)
θ	Contact angle ($^{\circ}$)
K_c	Thermal conductivity of copper ($\text{W}/\text{m.K}$)
Δx	Distance between thermocouple and condensation surface (mm)
t	Time (sec)
ρ	Liquid density (kg/m^3)
g	Acceleration due to gravity (m/s^2)
h_{lg}	Latent heat of evaporation (J/kg)
η	Liquid viscosity ($\text{N}\cdot\text{sec}/\text{m}^2$)
λ	Liquid thermal conductivity ($\text{W}/\text{m.K}$)
$\Delta\rho$	Density difference between vapor and condensate (kg/m^3)
L	Plate height (m)
d	Tube diameter (m)
u_{∞}	Free-stream vapor velocity (m/s)
Nu_d	Nusselt number
Re_d	Reynolds number
R	Specific ideal-gas constant
γ	Ratio of the principal specific heat capacities
v_f	Specific volume of the saturated liquid

K_1	Dimensionless constant
K_2	Promoter-dependent dimensionless constant
K_3	Constant
r	Radius of a drop
\hat{r}	Radius of the largest drop
\check{r}	Radius of the smallest drop
DWC	Dropwise condensation
FWC	Filmwise condensation
SAM	Self-assembled monolayers
PTFE	Polytetrafluoroethylene

CHAPTER 1: INTRODUCTION

Condensation of vapor has critical engineering importance due to its widespread application in numerous industrial processes. Condensation is the change of physical state of matter from gaseous phase to liquid phase. Condensation occurs whenever a vapor comes into contact with a surface at a temperature lower than the saturation temperature corresponding to its vapor pressure. Two distinct forms of condensation are observed:

- Dropwise condensation
- Film wise condensation

1.1 Dropwise condensation

Dropwise condensation, characterized by countless droplets of varying diameters on the condensing surface instead of a continuous liquid film as shown in figure 1.1, is one of the most effective mechanisms of heat transfer, and extremely large heat transfer coefficients can be achieved with this mechanism. In dropwise condensation, the small droplets that form at the nucleation sites on the surface grow because of continued condensation, coalesce into large droplets, and slide down when they reach a certain size, clearing the surface and exposing it to vapor. There is no liquid film in this case to resist heat transfer. As a result, with dropwise condensation, heat transfer coefficient can be achieved that are more than 10 times larger than those associated with film condensation. Large heat transfer coefficients enable designers to achieve a specified heat transfer rate with a smaller surface area, and thus a smaller (and less expensive) condenser. Therefore, dropwise condensation is the preferred mode of condensation in heat transfer applications.



Figure 1.1: Dropwise condensation

The challenge in dropwise condensation is not to achieve it, but rather, to sustain it for prolonged periods of time. Dropwise condensation is achieved by adding a promoting chemical into the vapor, treating the surface with a promoter chemical, or coating the surface with a polymer such as Teflon or a noble metal such as gold, silver, rhodium, palladium, or platinum. The promoters used include various waxes and fatty acids such as oleic, stearic, and linoic acids. They lose their effectiveness after a while, however, because of fouling, oxidation, and the removal of the promoter from the surface. It is possible to sustain dropwise condensation for over a year by the combined effects of surface coating and periodic injection of the promoter into the vapor. However, any gain in heat transfer must be weighed against the cost associated with sustaining dropwise condensation.

1.2 Filmwise condensation

In film condensation, as shown in figure 1.2 the surface is blanketed by a liquid film of increasing thickness, and this “liquid wall” between solid surface and the vapor serves as a resistance to heat transfer. The heat of vaporization released as the vapor condenses must pass through this resistance before it can reach the solid surface and be transferred to the medium on the other side. Dropwise condensation is the preferred mode of condensation in heat transfer applications, and people have long tried to achieve sustained dropwise condensation by using various vapor additives and surface coatings. These attempts have not been very successful, however, since the dropwise condensation achieved did not last long and converted to film condensation after some time. Therefore, it is common practice to be conservative and assume film condensation in the design of heat transfer equipment.

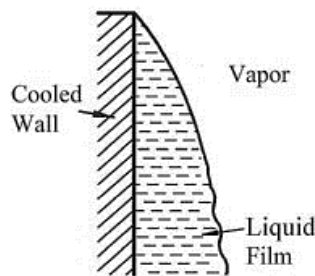


Figure 1.2: Filmwise condensation

1.3 Nucleation in vapors

When the pressure of the vapor is less than, equal to, or greater than that of the liquid at the given temperature, it is said to be undersaturated, saturated, or supersaturated with respect to the liquid phase. Although the first two conditions are thermodynamically stable, the supersaturated vapor is unstable. When supersaturated vapor comes into contact with liquid phase, condensation on the liquid occurs immediately. If no liquid is present, large supersaturations can be maintained for seconds at a time. The degree of supersaturation or super-saturation ratio, S , is defined as the ratio of the actual vapor pressure to the saturation pressure at the same temperature. When saturated vapor is expanded adiabatically, the saturation pressure in most cases falls more rapidly than the pressure of the vapor and the vapor becomes supersaturated. If ions or dust particles are present, liquid droplets will form on these impurities after only a small expansion, characteristically some 10-20% in the case of ions, and this is called heterogeneous nucleation. Higher expansions of greater supersaturation may be obtained when ions or contaminants are removed from the system, until suddenly a fog forms upon further increase in supersaturation. The formation of fog droplets is caused by the random absorption and evaporation of single molecules, which results in the formation of clusters of molecules. This is referred to as homogenous nucleation or self-nucleation. Homogeneous nucleation is a rare occurrence. A heterogeneity, such as an accommodating substrate surface, is almost always used to stimulate nucleation processes.

1.3.1 Heterogeneous nucleation in vapors

Condensation is usually started by removing heat via the walls of the structure containing the vapors to be condensed. The vapor near the wall can be cooled below its equilibrium saturation temperature for the specific system pressure if enough heat is removed. The creation of a liquid embryo at the interface between a metastable supersaturated vapor and another solid phase is one type of heterogeneous nucleation, as the heat removal process will create a temperature field with the lowest temperature directly at the contaminant's wall. If the solid surface is idealized as being perfectly smooth, in general, the shape of a droplet at the surface will be dictated by the shape

of the surface itself, the interfacial tension and the contact angle. For a flat solid surface, the embryo liquid droplet will have a profile like that shown in figure 1.3.

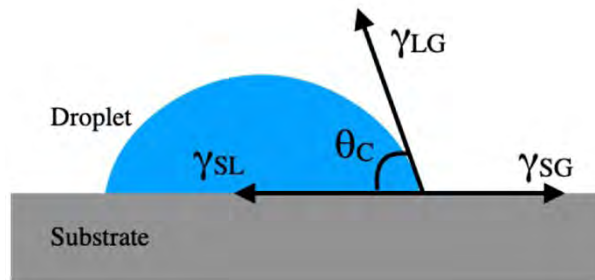


Figure 1.3: An embryo liquid droplet formed at an idealized liquid- solid interface

Where γ_{SL} , γ_{SG} and γ_{LG} denotes the interfacial tension between liquid and solid surface, surface free energy and surface tension force between liquid and gas respectively.

1.4 Factors affecting condensation heat transfer

Researchers are still looking for and studying elements that influence condensation behavior. The following sections examine the effects of pressure, surface sub-cooling, heat flow, non-condensable gases, vapor velocity, droplet characteristics, surface inclination and properties, and working fluids.

1.4.1 Vapor pressure

For a fixed temperature differential between the vapor and condensing surface, increasing vapor pressure increases heat flux and heat transfer coefficients. On the one hand, the decrease in interfacial resistance at the liquid-vapor interface [1] is responsible for this. This resistance results from a net movement of molecules from the surface, resulting in a slight temperature differential between the liquid's surface and the vapor, which is a few mean free pathways away. Increases in steam pressure, on the other hand, cause a fall in condensate surface tension, which affects wettability [2]. Tanner *et al.* [3], Stylianou and Rose [4], Shigeo and Hiroaki [5], and Kananeh *et al.* [6] are only a few of the researchers that have reported comparable findings. Wen *et al.* [7] also demonstrated how nucleation density and growth rate alter as pressure changes. At lower pressures, large radius drops covered a larger portion of the surface, obstructing heat transfer due to a reduction in effective heat transfer area.

1.4.2 Heat flux

In contrast to the patterns in filmwise condensation, Tanner *et al.* [3] discovered that the heat transfer coefficient increases with increasing heat flux for dropwise condensation. Graham and Griffith [8] gathered experimental data from earlier researchers and found that when the heat flux increased, the heat transfer coefficient initially increased and subsequently approximated a constant value. However, experiments by Utaka *et al.* [9] reveal that the heat transfer coefficient for organic fluids has a weak influence on heat flow. Bonner [10] proposed that the heat transfer coefficient of steam is heat flux dependent, but the heat transfer coefficient of organic fluids is independent. He also developed two separate heat transfer coefficient models, each of which he demonstrated to be consistent with earlier experimental evidence.

1.4.3 Surface Sub-cooling

Surface Sub-cooling is the difference between saturated vapor temperature and surface temperature. The heat flux for both DWC and FWC increases as subcooling increases. Heat fluxes, on the other hand, are substantially larger for DWC. The difference between the two modes is more noticeable at lower subcooling. Miljkovic *et al.* [11] used jumping droplets to demonstrate the same thing. DWC had a larger heat flux than FWC for a given degree of subcooling. The DWC surface got flooded as the temperature difference rose, and the performance plummeted to that of FWC. Graham [12] discovered that as subcooling increases, the heat transfer Co-efficient increases. Due to the increased number of active nucleation sites at high Sub-cooling, the heat transfer coefficient tends to remain constant [13].

1.4.4 Non-condensable gases

Non-condensable gases tend to clump together at the condensing surface, posing a major heat and mass transfer barrier. Tanner *et al.* [3] discovered that the presence of non-condensable gases slowed the rate of heat transfer in DWC compared to the absence of these gases. The magnitude of the reduction was determined by the heat flow at the surface and the steam pressure. Non-condensable gases, even in minute amounts, have a high thermal resistance [12-14]. Early scientists clearly proved the effect of non-condensable, but no quantitative measurements for dropwise

condensation experiments were documented. McNeil *et al.* [15] experimented with pure steam as well as steam mixed with 10,000 ppm of air. Even though the heat transmission rate dropped, it was still marginally better than in the filmwise mode, according to the researchers. Ma *et al.* [16] examined the heat transfer properties of DWC in the presence of non-condensable gases in an experimental setting. When compared to FWC, the interfacial dynamic interaction generated by droplet growth, coalescence, and departure resulted in a 30-80% increase in heat transmission. Ma *et al.* [17] describe experimental observations of DWC on super hydrophobic surfaces in the presence of non-condensable. In the presence of non-condensable gases (NCG), they examined the performance of a hydrophobic and a super hydrophobic surface. The hydrophobic surface has a larger heat flow than the super hydrophobic surface at low concentrations of NCGs. Super-hydrophobic surfaces, on the other hand, perform better when the concentration of NCG rises. This is explained by the NCG filling gaps between the micro pillars in the super hydrophobic surface, preventing the droplet from entering the Cassie state, which has more mobility and hence better heat transfer [18]. Thus, the experimental findings so far imply that the presence of NCGs reduces DWC's performance while maintaining its superiority over FWC under the same settings.

1.4.5 Vapor velocity

The effects of vapor velocity on condensation were initially studied by Tanner *et al.* [3] and Graham [12]. Both studies found that increasing vapor velocity improved overall condensation heat transfer by assisting in the removal of non-condensable and altering the flow of condensate. Their velocity readings were taken in the input pipes, and the exact values at the condensing surface were unknown. Although there is considerable agreement that vapor velocity affects droplet mobility on the condensing surface, experimental evidence to define the extent of the increase and its relationship to vapor velocity is sparse.

1.4.6 Droplet characteristics

Nucleation is an important process in most phase-change processes and involves the formation of initial fragments of a new phase from a metastable phase. These shards combine to generate drops. Mc-Cormick and Westwater [19] were the first to investigate drop nucleation in DWC, finding that drops formed on the condenser surface at imperfections. Graham and Griffith [8] used drop distribution measurements and constructed models to explain how droplet density and size influenced heat transmission characteristics. Tanasawa and Ochiai [20] used a high-speed camera to study the condensation of steam on a cylindrical surface and gained insight into droplet dynamics. They investigated the critical droplet radius at breakoff and discovered that the real critical radius differs significantly from that calculated using a basic static force balance of surface tension and gravity forces. A microscope was used to photograph the drop size distribution. Graham [12] and LeFevre and Rose [14] obtained distribution functions that were like other researchers. It was discovered that a higher percentage of smaller drops resulted in increased heat transmission. Leach *et al.* [21] investigated the nucleation and development of water drops on a natural convection-cooled substrate. Drop distributions, nucleation densities, growth and coalescence patterns are all presented. In the presence of tiny pillars, Narhe and Beysens [22] explored the dynamic condensation of steam on super hydrophobic surfaces and described nucleation, growth, and coalescence.

Depending on the surface energy difference, vapor condenses on the surface and either wets the surface or forms distinct droplets. The lower the substrate's surface energy, the more probable the vapor will condense into discrete droplets. The wettability of a surface is measured by the contact angle that corresponds to it, which is given by Eq. 1.1 [23] for an ideal surface:

$$\theta = \arccos\left(\frac{\sigma_{sv} - \sigma_{sl}}{\sigma_{lv}}\right) \quad (1.1)$$

Where θ denotes contact angle and σ_{sv} , σ_{sl} , σ_{lv} denote surface tension at solid-vapor interface, solid-liquid interface, liquid-vapor interface respectively.

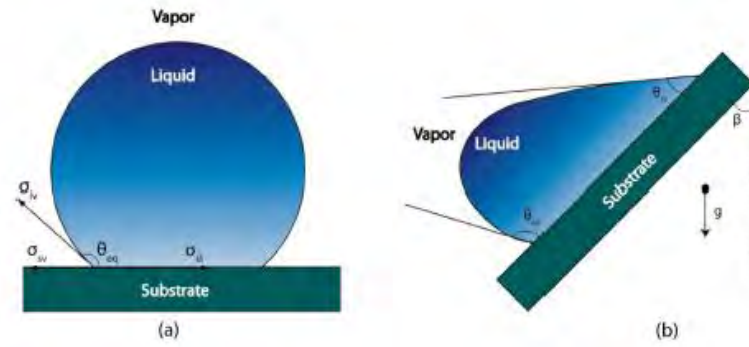


Figure 1.4: Schematic of static and dynamic contact angles

When the contact angle is more than 90 degrees, the surface is termed as hydrophobic and has poor wetting properties. A hydrophilic surface has a contact angle of less than 90 degrees. As a result, the surface wettability decreases as the contact angle increases, increasing dropwise condensation. Contact angle is influenced by several factors, including surface roughness, particle shape and size, heterogeneity, and so on. Surface roughness affects the growth rate and contact angle in a droplet because real or "nonideal" surfaces are not molecularly smooth. Both of Wenzel's and Cassie's morphologies can be seen when a genuine surface is wet. The roughness of many surfaces is characterized by the ratio of total surface area to projected area. The liquid droplet fully wets the rough surface in the Wenzel condition; the surface roughness intensifies the intrinsic wetting qualities. The droplet suspends over micro/nanostructures in the Cassie state. The partially moist stage is depicted in Figure 1.5. When a droplet does not spread but instead forms a spherical cap on the substrate, it is said to be partially moist.

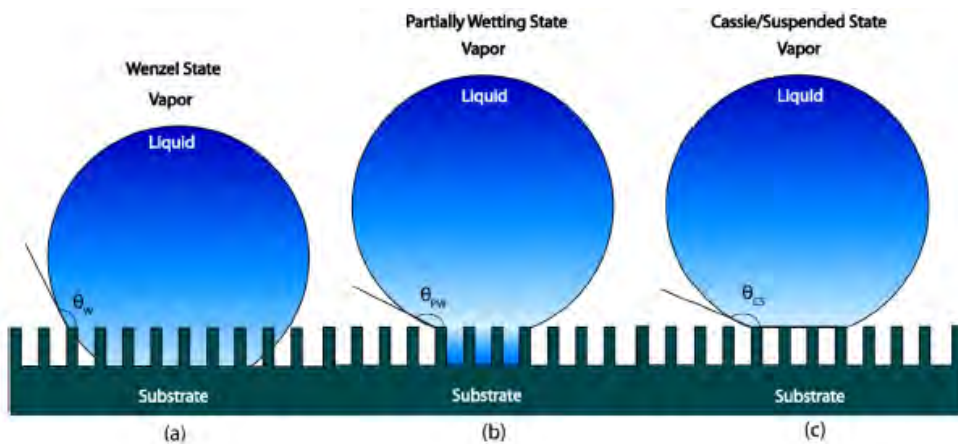


Figure 1.5: Schematic showing wetting regimes over rough surface (a) Wenzel state (b) Partially wetting state (c) Cassie-Baxter or Suspended state.

Walpot *et al.* [24] found that surfaces with larger contact angles may have inferior performance, contrary to predictions. When the contact angle was increased from 79° to 105°, smaller droplets formed, resulting in smaller drainage routes, which hampered heat transfer to a degree. The relevance of condensate drainage in these heat exchangers was highlighted in this study.

1.4.7 Surface properties

The surplus energy at the surface compared to its mass is referred to as surface energy. It can also be thought of as the effort necessary to transform a bulk into a surface. A low surface energy material is preferred for a heat transfer surface to prevent wetting and aid in the creation of droplets. Metals, which are commonly used in heat exchangers, have a high surface energy. To take advantage of metal's natural advantages in heat exchanger design and construction, different coatings or surface treatments must be considered to reduce surface energy and assure DWC. Graham [12] discovered that the nucleation density and droplet behavior were controlled by the surface finish. It was therefore critical to investigate surface properties and their implications for heat transport.

Previously, low-energy organic molecules such as dioctadecyl disulphide were employed to coat the surface [3, 25, 26]. Finding the appropriate balance was a major difficulty. A thicker coating ensured long-term adherence while also adding significant thermal resistance to counteract the dropwise condensation advantage.

Development of self-assembled monolayers (SAMs) has aided the construction of super hydrophobic surfaces. SAMs are organic molecule chains having functional groups attached at the ends. They are ideal promoter materials because of their poor heat resistance, strong hydrophobicity, and propensity to chemisorb on metals [27]. [2] demonstrated the use of SAMs on gold and copper surfaces and observed contact angles greater than 100°.

Researchers designed surfaces with grooves to promote condensate flow after modifying condensate mobility to improve heat transmission. Izumi *et al.* [28] looked

at vertical and horizontal surfaces with circular grooves and discovered that a groove width of 2 mm increased DWC by almost 25%. According to Peng *et al.* [29], groove orientation has a considerable impact on the performance of hydrophobic surfaces, although the effect is less noticeable for super hydrophobic surfaces.

Surfaces and their qualities have a huge impact on heat transfer. Researchers have attempted to create materials with improved heat transfer properties that are durable enough to withstand industrial use. Aside from the ways discussed above, some researchers are studying rare-earth ceramic oxides, which are both strong and hydrophobic by nature, and others are drawing inspiration from nature to produce bio-mimetic surfaces.

1.4.8 Surface inclination

Citakoglu and Rose [30] reported that droplet removal and hence the condensation rate is affected by inclination. Because the action of gravity to move droplets is more pronounced in vertical and face down postures, they observed that the highest condensation occurred. After conducting trials on two salinized surfaces at varying inclinations, Liao *et al.* [31] determined that surface inclination has a considerable impact on heat transfer findings, with bigger inclination resulting to increased condensation by as much as 100%. The droplet departure size can be used to explain this. Smaller droplet departure sizes arise from larger inclinations, resulting in a faster rate of heat transfer.

1.4.9 Working fluids

The majority of dropwise condensation research has concentrated on improving steam condensation. Steam is being researched more closely for two reasons: its ease of forming drops due to its high surface tension and its broad industrial use. Condensation of other fluids like refrigerants and organic fluids, on the other hand, is of interest. Working fluids such as ethylene glycol, aniline, nitrobenzene, propylene glycol, glycerol, ethanol, hexane, and others have been studied on various condensing surfaces, according to the literature.

1.5 Applications of condensation heat transfer

Dropwise condensation has a higher heat transfer coefficient, but it's worth noting that the fundamental issue in applying dropwise condensation in industry has been, and continues to be, the reliability of fostering dropwise condensation over a long period of time in difficult conditions (rather than under controlled lab conditions). The usefulness of condensation heat transfer for diverse end users is examined further in the next section, with a focus on practicality.

1.5.1 Power generation

Almost all steam driven power plants (Rankine and combined cycles) have a condenser downstream of the steam turbine. Condensation is achieved using liquid-coupled shell-and-tube condensers, evaporative cooling towers, or air-coupled condensers. Condensation can occur on both the shell and tube sides of shell-and-tube devices. Given that these steam handling systems typically have high volumetric flow rates, placing the vapor on the shell-side can help reduce pressure loss through correct design optimization. Furthermore, the cooling water is retained on the tube side to reduce the effects of corrosion. As a result, the condensation of steam on the outside surfaces of tubes is of great importance.

1.5.2 Desalination

Desalinated water is used by most water stressed regions to augment their water supply. The total capacity is produced by membrane processes (64%) and thermal processes (36%) [32]. More than 90% of all thermal desalination systems are multi-stage flash, multiple effect distillation, and thermal vapor compression [33]. The salt water is evaporated, and the condensate is collected in these methods. Shell-and-tube condensers or plate heat exchangers are commonly used for condensation. In these condensers, dropwise condensation could result in higher heat transfer rates and smaller heat transfer regions, lowering capital costs. According to Lukic *et al.* [34], the unit cost of water production can be decreased by up to 35%. Because of its scalability, lowering the cost of these technologies can have a big impact.

1.5.3 Refrigeration and air-conditioning

Condensers, commonly finned-tube condensers, are used in standard heating, ventilation, and air-conditioning (HVAC) systems to reject heat to the ambient. These air-coupled condensers, like the air-coupled condensers used in power plants, are limited by air-side heat transfer. Condensed ambient water that collects on cooling coils can obstruct heat transfer in air conditioners, potentially resulting in poor cooling efficiency and pathogen growth. Engineered surfaces that encourage DWC, and quick condensate shedding have recently been proposed to increase overall condenser performance by lowering the amount of condensed water [35] on fin and tube surfaces.

1.5.4 Electronics thermal management

As electronic devices continue to require higher processing capabilities in smaller volume, overall power and heat flux dissipation has increased significantly. Thermal management is essential in such systems to keep the device's core temperatures at the proper levels. The electronics industry's cooling requirements have outstripped the heat dissipation rates achievable by traditional air-cooled systems. Microchannel heat sinks, jet impingement cooling, and phase-change based technologies like heat pipes, thermosiphons, and vapor chambers are all becoming more popular [36]. An evaporator, in which the working fluid boils as heat is given to it, a condenser, in which the working fluid condenses and rejects heat to the ambient, and a return mechanism, in which the condensate is returned to the evaporator.

1.5.5 Petrochemical refining

Fractional distillation of crude oil produces petroleum products, which involves the evaporation and condensation of various crude oil components. Water is commonly utilized as the cooling medium in condensers. Rose [1] reviewed dropwise condensation technologies and suggested that they could be used in petroleum refining.

1.5.6 Water harvesting

Most water harvesting methods require condensation and then water transport away from the surface of capture. Lee *et al.* [37] investigated the impact of surface wettability on water harvesting rates.

1.6 Motivation for the work

Condensation is the change of physical state of matter from gas phase into liquid phase. Condensation occurs when the temperature of a vapor is reduced below its saturation temperature. This is usually done by bringing the vapor into contact with a solid surface whose temperature is below the saturation temperature of the vapor. But condensation can also occur on the free surface of a liquid or even in a gas when the temperature of the liquid or the gas to which the vapor is exposed is below the saturation temperature. Condensation is widely used in many industrial applications such as power plants [38], refrigeration and air-conditioning system [39], water desalination [40], dehumidification [41], petroleum industry, chemical production plant, etc. Condensation heat transfer occurs in two modes i.e., dropwise condensation and filmwise condensation. In film condensation, the condensate wets the surface and forms a liquid film on the surface that slides down under the influence of gravity. The thickness of the liquid film increases in the flow direction as more vapor condenses on the film. As the film thickness increases it reduces the heat transfer coefficient. In dropwise condensation, the condensed vapor forms droplets on the surface instead of a continuous film and the surface is covered by countless droplets of varying diameters. With dropwise condensation, heat transfer coefficients can be achieved that are more than 10 times larger [42-46] than those associated with film condensation. But it is extremely difficult to maintain dropwise condensation since most surfaces become wetted after exposure to a condensing vapor over an extended period.

Heat transfer performance depends on heat transfer coefficient. Any modification in the condensation phenomenon, which improves heat transfer performance, decreases pumping power, or reduces condensers size. These outcomes consequently reduce manufacturing or operating costs and increases efficiency.

Condensation behavior depends on many factors including surface morphology, material, degree of sub-cooling, characteristics of the fluid, etc. Among those properties surface modification is an easy and effective way to improve the condensation behavior. Adoption of grooves on a surface could minimize the resistance that the droplet face when sliding during condensation.

Here, an experiment is carried out to improve the condensation behavior by introducing various micro-grooves (rectangular, sinusoidal, and wedge-shaped micro-groove) on the flat copper plate thus increasing the heat transfer coefficient and therefore increasing the condensation performance.

1.7 Objectives

The objectives of the present work can be summarized as follows:

- To study the surface morphological effect on condensation behavior.
- To study and analyze the condensation behavior (droplet nucleation process, droplet size, distribution and frequency of droplet, drainage rate) on the modified surface and compare it with plain copper surface.
- To assess the most effective micro-grooved surface in condensation among the various surface modifications applied in this study based on condensation heat transfer rate.

1.8 Layout of the thesis

The study presented in this dissertation has addressed “Effect of Micro Groove on Condensation Behavior of Vertical Copper Plate”. The dissertation has been organized as follows. In chapter 1, a general discussion on condensation heat transfer, application of condensation heat transfer and the factors that affect condensation heat transfer has been discussed. In chapter 2, a detail literature review, and a brief discussion on the evolution of different condensation model have been presented for a better conception in previous studies regarding condensation heat transfer on different surfaces. In chapter 3, a brief discussion on droplet nucleation process has been discussed. In chapter 4, discussion about the design of experimental setup, data acquisition system, data analysis and uncertainty analysis has been done. In chapter 5, the experimental results have been discussed. Finally, in chapter-6, conclusion and recommendation for further improvements have been discussed.

CHAPTER 2: LITERATURE REVIEW

Current chapter aims to provide a review of several experimental, analytical, and numerical investigations on condensation heat transfer made by researchers during a couple of decades.

2.1 Existing literature on condensation

Among different parameters, the nucleation density, or the number of active nucleation sites, affects the mode of condensation heat transfer. The creation of a liquid film at the condensing surface is aided by a higher nucleation density, which improves the transition from dropwise to filmwise condensation. As a result of the formation of a liquid film during filmwise condensation, it provides heat resistance [47] and prevents the formation of new heterogeneous nucleation sites. Nucleation density also depends on surface morphology. Surfaces that are more wettable (i.e., hydrophilic) has higher nucleation density than hydrophobic surfaces [42]. As a result of the increased nucleation density, super hydrophilic surfaces tend to produce liquid films on condensing surfaces, which can then be employed for liquid condensate drainage.

The contact angle affects surface wettability as well. When the contact angle is more than 90 degrees, the surface is considered poor wetting and is referred to as hydrophobic. A contact angle of less than 90 degrees defines a hydrophilic surface. As a result, as the contact angle increases, the surface wettability diminishes, promoting dropwise condensation. Recent advancements in surface science [48-51] have reignited interest in fine-tuning surface wettability to promote and maintain DWC. Because of their great droplet mobility (i.e., minimal contact angle hysteresis), super hydrophobic surfaces have become a preferred choice for gravity-induced condensate shedding. Droplet removal reduces liquid conductive thermal resistance, enhancing HTC, and shedding a condensate droplet at a smaller size is favorable for DWC. Many parameters, including surface roughness, particle shape and size, heterogeneity, and so on, influence contact angle and surface wettability [52]. Orlova *et al.* [53] examined the contact angle of water on copper surfaces and demonstrated how surface roughness, microstructure, and flow rate affect contact angle.

Although super hydrophobic surfaces perform better in DWC than surfaces with higher wettability (e.g., hydrophobic, hydrophilic, or super hydrophilic), this is not always the case. For example, compared to more wettable surfaces, super hydrophobic surfaces have a higher thermodynamic barrier to nucleation, which may result in lower condensation rates [1, 10]. As a result, super hydrophobic surfaces may have inferior DWC heat transfer performance than hydrophobic surfaces [54]. To address this problem, other surface types have been proposed, including hydrophilic–hydrophobic patterned surfaces [55-57], hybrid surfaces [50, 58, 59], wettability gradient surfaces [60], grooved surfaces [28], and so on.

On the hybrid-patterned surface, dropwise and filmwise condensations coexist in separate stripe-regions. Droplets in the dropwise condensation area can merge with the liquid film on the hydrophilic surface and travel to the filmwise condensation region. As a result, the maximum droplet size can be modified by changing the hybrid surface's structure. Ghosh *et al.* [61] created hybrid-patterned surfaces inspired by the banana leaf to absorb water from humid air, and they inter-spaced 300 or 400 μm wide filmwise condensation tracks to adjust the stripe width for dropwise condensation from 400 to 2500 μm . They showed a 19 percent increase in condensate collection and a 20 percent increase in heat transfer coefficient.

Accelerated surface rejuvenation process can also improve the condensation behavior. The surface rejuvenation process can be accelerated by increasing the droplet sliding velocity, which improves condensation heat transfer behavior. Droplets originate on active nucleation sites then they grow and shed by gravity. As droplets fall from the surface, they mix with other droplets in their route, clearing the surface of droplets and exposing the surface, which stimulates droplet production. Dropwise condensation is greatly affected by the sweeping cycle and droplet departure diameter, according to research into condensation behavior. Tanasawa *et al.* [62] found that when droplet sizes increased, the heat transfer coefficient decreased. Microgrooves can be introduced on condensing surfaces to improve heat transfer efficiency. Microgrooves on the condensing surface can substantially minimize the resistance and adhesion work

of droplets sliding, making them a simple and practical approach for improving dropwise condensation heat transfer behavior. Watanabe *et al.* [63] initially indicated that creating micro-grooves on super hydrophobic surfaces can greatly lower the sweeping cycle and departure diameter of falling droplets. Photolithographic approaches for introducing micro designs on aluminum surfaces with parallel grooves were explored by Sommers and Jacobi [64]. The crucial droplet size on micro-grooved surfaces was roughly 50% smaller than on the identical surface without micro-grooves, according to their findings. In comparison to a vertically oriented non-textured hydrophobic surface, Dietz *et al.* [65] predicted that a vertically oriented super hydrophobic surface should deliver a 100 percent increase in the DWC heat transfer coefficient. Under modest subcooling, super hydrophobic surfaces can even cause self-propelled jumping droplets, which help remove condensate formed on such low-energy surfaces [66]. However, at greater surface subcooling temperatures, this phenomenon is not observed [67].

Li *et al.* [68] investigated the sliding of falling droplets on micro-V grooves of various pitches. The contact angle of droplets rose as the groove depth and V-angle increased in the experiments. The increase in groove pitch aided the sliding of droplets, and the wetting behavior was clearly anisotropic. To improve the dropwise condensation heat transfer behavior, Zamuruyev *et al.* [69] constructed micro-scale trapezoidal grooves on the hydrophobic surface. Their experiments revealed that micro-grooved surfaces can improve droplet transfer from the Wenzel to Cassie states, and that these trapezoidal grooves formed a capillary pressure gradient, allowing droplet transfer from the condensing surfaces. Lu and his colleagues constructed a theoretical model [70] to predict the efficiency of dropwise condensation heat transfer for surfaces with microscopic triangular grooves, and the calculated findings matched their experimental results as well. Lara and co-workers [71] studied the effects of semicircular groove size on dropwise condensation heat transfer. Their experimental results showed that a greater heat flux was obtained on the smaller sizes of semicircular groove. The sweeping effects of falling droplets were increased 30-50 percent for sinusoidal shaped micro-grooved plate compared to flat plate, according to Xiang Li and colleagues [72]. Peng *et al.* [29] have studied the influence of groove orientation

and shown that the hydrophobic surface with vertical microgrooves had 21–58% higher condensation heat transfer coefficient than hydrophobic surface with horizontal microgrooves. Effects of groove on natural water harvesting system had come to focus then. Malik *et al.* [73] and Norgaard *et al.* [74] have showed that surfaces of some plants are able to harvest water from atmosphere. Several attempts have been made to mimic the mechanisms observed in nature [75]. Leaf vein structures were used earlier [61], [56] to show the effective transport of liquid droplets.

However, Condensation behavior on wedge shape (leaf vein structure) micro-grooved copper plate is yet to be studied. Effect of rectangular-shaped microgroove is also needed to be explored. Surface wettability and heat transfer behavior of sinusoidal-shaped micro-grooved copper plate is also needed to be investigated. So, it is one of the prime goals of the present study to investigate the effect of microgroove on condensation heat transfer.

2.2 Condensation heat transfer model

When a liquid and its vapor are in contact, molecules pass from liquid to vapor and from vapor to liquid. When the number of molecules entering the liquid phase exceeds the number of molecules exiting, condensation occurs. The temperature of the vapor in the immediate region of the vapor-liquid interface (a few mean free pathways) is higher than that of the liquid in these conditions. The temperature drop at the interface increases as the condensation rate and pressure decreases, although in most cases (except for liquid metals), this is extremely minor, and equilibrium conditions at the interface can be assumed.

Experimental, computational, and theoretical investigations on hydrodynamics and heat transmission during condensation can be found in the open literature. For example, one of the well-known classical techniques developed in 1916 is Nusselt's [76] theory for film-wise condensation mode, whereas Rose's [1] correlation for dropwise condensation mode is widely used to assess the thermal performance of vapor-to-liquid phase change. Filmwise condensation is commonly understood by modelling a liquid sheet as a thermal barrier between vapor and a subcooled wall

utilizing laminar wave-free film flow. Dropwise condensation, on the other hand, is still a hot topic among scientists. DWC models with a more complicated set of equations and parameters, such as liquid wall contact angle, drop size distribution, critical droplet diameter, and nucleation density [77], have been constructed. Experimental data for DWC and FWC on coated unstructured surfaces covered with SAM, PTFE, spin-coated, chemically etched, or treated with polymer-based agents is used to build certain mathematical techniques. Others include variables such as liquid–solid interfacial thermal conductivity or vapor atom accumulation coefficient on liquid layer, both of which have been thoroughly analyzed using molecular dynamics [78] or empirical analysis. The more parameters the models include, the more precise and powerful the calculations for DWC become, but the more complicated analysis is required. When considering either of the condensation modes, the thermo-hydrodynamic behavior can be better managed. The complexity of predicting overall thermal performance increases in the case of vapor-to-liquid phase-change propagating in the transition mode known as drop-film wise condensation (DFWC), because this mode is governed by a sequence of droplet initiation, their subsequent random accumulation, and possibly rivulet formation. DFWC mode is frequently observed, especially when micro structured surfaces are used for heat transfer enhancement in heat exchangers or condensers. The following sections examine Nusselt's model for film condensation and Rose's correlation for dropwise condensation.

2.2.1 Nusselt's model

Nusselt's main assumptions are that heat transfer across the condensate film is by pure conduction, the effect of vapor drags in supporting the falling condensate film is negligible, and the properties of the condensate may be taken to be uniform across the film, i.e., are essentially independent of temperature.

The well-known Nusselt equations are:

For the vertical plane surface, the mean value of Nusselt number is

$$\text{Nu} = 0.943 \left\{ \frac{\rho \Delta \rho g h_{1g} L^3}{\eta \lambda \Delta T} \right\}^{1/4} \quad (2.1)$$

And for the horizontal tube

$$\text{Nu} = 0.728 \left\{ \frac{\rho \Delta \rho g h_{lg} d^3}{\eta \lambda \Delta T} \right\}^{1/4} \quad (2.2)$$

Where ρ is the liquid density, g is acceleration due to gravity, h_{lg} is the latent heat of evaporation, η is the liquid viscosity, λ is the liquid thermal conductivity, $\Delta\rho$ is the density difference between vapor and condensate, ΔT is the vapor-to-surface temperature difference; L is the plate height; and d , the tube diameter. For the case of the tube, the additional assumption that film thickness is small compared to the tube radius is needed. Since the theory predicts that the radial film thickness tends to infinity at the bottom of the tube, this assumption is evidently invalid for the lower part of the tube. The fact that the heat transfer rate is inaccurate where the film becomes thick is relatively unimportant because it is small and makes a minor contribution to the total heat transfer rate for the tube. Equations (2.1) and (2.2) have been well verified experimentally for condensation of pure (only one molecular constituent) vapor. To obtain the constant in Eq. (2.2), numerical integration is required twice. Nusselt's slightly inaccurate value $(0.8024 (2/3)^{1/4} = 0.725)$ is due to his use of planimetry.

More recent theoretical studies, as mentioned by Rose [79], have revealed that the effects of inertia and convection in the condensate layer, as well as vapor drag on the condensate surface, are insignificant. Memory and Rose [80] have recently proven that the influence of fluctuating wall temperature, which occurs in practice during condensation on a horizontal tube, has no effect on the mean heat transfer rate. When the condensate flow is laminar, equation (2.1) and (2.2) can be applied with confidence for condensation of pure "stationary" vapors.

The influence of drag on the condensate becomes significant when the vapor flow rate over the condensing surface is high. In some cases, the influence of vapor drag outweighs the effect of gravity. The consequences of vapor shear stress have been intensively investigated since 1960. Rose [79] describes some of the more significant contributions.

The relative importance of vapor shear stress and gravity on the motion of the condensate film is measured by the dimensionless parameter $F = \eta h_{lg} g x / \lambda \Delta T u_{\infty}^2$, where x is the relevant linear dimension (plate height or tube diameter) and u_{∞} is the free-stream vapor velocity. For downward vapor flow over a horizontal tube, an approximate analysis gives

$$\text{Nu}_d \text{Re}_d^{-1/2} = \frac{0.9 + 0.728F^{1/2}}{(1 + 3.44F^{1/2} + F)^{1/4}} \quad (2.3)$$

Nu_d is the mean Nusselt number for the condensate film and Re_d is a Reynolds number using the vapor approach velocity and condensate properties. Equation (2.3) which indicates that for $F > 10$, gravity dominates while for $F < 0.1$, vapor shear stress is controlling; agrees quite well with experimental data from several investigations using various condensing fluids.

2.2.2 Background mechanism of dropwise condensation modeling

The heat transfer rates related with dropwise condensation have been estimated/modeled in a variety of ways. The three unique mechanisms of dropwise condensation that have been modeled in the literature [81-83]. When vapor condenses between droplets in practically droplet-free zones, the first process occurs. Surface diffusion takes place within the adsorbed coating and transports the condensate to the droplets. Because of the thin boundary layer thickness, the conduction heat transfer resistance may usually be ignored. Heat transfer happens in the extremely thin liquid film and at discrete droplets, according to this hypothesis. Vapor condenses in the filmwise mode in the second mechanism, generating a very thin film at first. Due to interfacial instabilities, the liquid film ruptures when it reaches a critical thickness, and minute droplets form. The condensate film is primarily responsible for heat transfer, whereas droplets are considered liquid collectors. This paradigm was first proposed by Jakob [84]. Due to their strong parallels, some researchers have merged these two systems in their models [85-87]. The nucleation theory provides the basis for the third modeling framework. At active nucleation sites like pits and grooves, vapor condenses into distinct droplets, according to this hypothesis. At the atomic level, droplets form and grow into the continuum [83] domain. Heat transfer happens exclusively at the

droplets, which is normally restricted by their heat conduction resistance, and the section of the surface between growing drops remains dormant. Eucken [88] proposed this concept originally, and it has since been improved and updated by various scholars. In the realm of dropwise condensation, this is the most used model.

Commonly used assumptions in the literature for model development that simplify the physical phenomena while capturing the required details are listed below:

- Nucleation sites follow a random spatial distribution.
- The minimum radius of a droplet is constrained by the smallest thermodynamically determined droplet radius.
- The substrate is assumed to be initially bare, and all the nucleation sites are instantaneously occupied by droplets of having minimum radius.
- The entire substrate is at uniform temperature. Any local variation due to variations in droplet dynamics is neglected.
- The presence of non-condensable is usually not accounted for.

Many models were developed based on thermal resistances due to the liquid-vapor interface, droplet curvature, and conduction in the droplet driven by the subcooled substrate.

2.2.3 Correlation of Rose for dropwise condensation

Le Fevre and Rose's idea [14] was later found to be in good agreement with data for steam throughout a wide range of heat flux and vapor pressure, as well as data for other fluids (see, for instance, Rose [14] and Rose *et al.* [89]). The basic idea is to combine a formula for heat transfer through a given size drop with an expression for the average distribution of drop sizes, then integrate overall drop sizes to get the heat flux for the surface for a given vapor–surface temperature differential. Conduction, surface curvature, and the temperature drop at the contact are all important components in the equation for heat transfer through a drop (matter transfer resistance). Tanaka [90] takes a similar technique and goes into great length about the coalescence process. In the theory of Le Fevre and Rose [14] the heat flux through the base of a hemispherical (a good approximation for water) drop with radius r is given by

$$q_b = \frac{\Delta T - \frac{(2\sigma T_{sat})}{(r\rho_f h_{fg})}}{K_1 \frac{r}{k} + K_2 \left(\frac{0.627}{0.664}\right) \frac{T_{sat}}{(h_{fg}^2 \rho_g)} \frac{(\gamma+1)}{(\gamma-1)} \left[\frac{(RT_{sat})}{2\pi}\right]^{1/2}} \quad (2.4)$$

(Note that equation (2.4) has been slightly modified by introduction of the factor 0.627/0.664 (see Rose [91]) from that originally used by Le Fevre and Rose [14]).

The second term in the numerator on the right-hand side of equation (2.4) is the amount by which the vapor must be subcooled to condense on the convex liquid surface. The first term in the denominator is the conduction resistance, and the second term accounts for interphase matter transfer as well as possible promoter layer resistance (included in K_2). For the distribution of drop sizes, Le Fevre and Rose [14] used

$$f = 1 - \left(\frac{r}{\hat{r}}\right)^{1/3} \quad (2.5)$$

Where f is the fraction of surface area covered by drops having a base radius greater than r . Equation (2.5) indicates that no area is covered by drops larger than the largest, and that, as the drop radius approaches zero, the fraction of area covered by all larger drops approaches unity. Equation (2.5) may be written as

$$A(r)dr = \frac{1}{3} \left(\frac{r}{\hat{r}}\right)^{1/3} \frac{dr}{\hat{r}} \quad (2.6)$$

Or

$$N(r)dr = \frac{1}{3\pi r^2} \left(\frac{r}{\hat{r}}\right)^{1/3} \frac{dr}{\hat{r}} \quad (2.7)$$

Equations (2.2) and (2.4) were combined and the average heat flux for the surface (in terms of the temperature difference) was obtained by integration over all drop radii:

$$q = \frac{1}{3\hat{r}^{1/3}} \times \int_{\check{r}}^{\hat{r}} \left\{ \frac{T - \frac{(2\sigma T_{sat})}{(r\rho_f h_{fg})}}{K_1 \frac{r}{k} + K_2 \left(\frac{0.627}{0.664}\right) \frac{T_{sat}}{(h_{fg}^2 \rho_g)} \frac{(\gamma+1)}{(\gamma-1)} \left[\frac{(RT_{sat})}{2\pi}\right]^{1/2}} \right\} \times r^{-2/3} dr \quad (2.8)$$

Where the minimum drop radius is taken to be that of the smallest viable (thermodynamically) drop

$$\check{r} = \frac{2\sigma v_f}{h_{fg}\Delta T} \quad (2.9)$$

And the maximum, based on dimensional analysis, is taken as

$$\hat{r} = K_3 \left[\frac{\sigma}{\rho g} \right]^{1/2} \quad (2.10)$$

The theory was initially criticized for having four seemingly adjustable constants, two (K_1 and K_2) in equation (2.4), one in the expression for the drop size distribution [the index 1/3 in equation (2.5)] and one in equation (2.10) K_3 , which were chosen to fit the available reliable data for steam at atmospheric pressure. All the constants, on the other hand, were known to be near to unity, and three of them could have been calculated independently.

The different types of models for dropwise condensation have been proposed. They are widely known as the first model and second model.

2.2.4 First model

The first model is based on the premise that droplet formation is a heterogeneous nucleation process like that described in section 1.3.1 Droplet embryos are postulated to form and grow at the nucleation sites, while portions of the surface between the growing droplets remain dry [46]. This type of model apparently was first proposed by Eucken [88] in 1937. Experimental evidence supporting this physical model of the condensation process has emerged from several experimental investigations.

In an early study, McCormick and Baer [19] presented experimental results supporting the contention that microscopic droplets are nucleated at active nucleation sites on the cooled surface. These active sites were identified as wetted crevices and grooves in the surface that were repeatedly reexposed to super-saturated vapor as a result of the coalescence of droplets and their removal from the surface by drag or gravity body forces. Using an optical technique to indicate changes in the thickness of very thin liquid films, Umur and Griffith [83] found that, at least for low temperature differences, the area between growing droplets on the surface was in fact dry. Their results indicate that no film greater than a monolayer existed between the droplets, and that no condensation took place in those areas. A model of dropwise condensation process that includes droplet nucleation, growth, removal, and renucleation on reexposed sites was developed by Gose *et al.* [92].

2.2.5 Second model

In this model, it is postulated that condensation occurs initially in a filmwise manner, forming an extremely thin film on the solid surface. As condensation continues, this film eventually reaches a critical thickness, estimated to be about 1 μm , at which point it ruptures and droplets form. Condensation then continues on the surface between the droplets that form when the film ruptures. Condensate produced in these regions is drawn to adjacent drops by surface-tension effects. Droplets also grow by direct condensation on the droplet surfaces themselves.

The second model of the dropwise condensation process apparently was proposed by Jakob [84] as early as 1936. Modified versions of this model have also been proposed by Silver [93]. The results of several investigations seem to be supported this type of interpretation of the condensation process. Results presented by Welch and Westwater [86] and Sugawara and Katsuta [87] indicate that condensation occurs entirely between droplets on a very thin liquid film. Welch and Westwater [86] observed the process by taking high speed movies through a microscope. It appeared to them that droplets large enough to be visible grew mainly by coalescence, leaving behind a “lustrous bare area,” which quickly took on a faded appearance. They interpreted the lustrous appearance as corresponding to thin film, which, upon rupturing at a thickness of around 1 μm , took on a more dull appearance.

CHAPTER 3: EXPERIMENTAL PROCEDURE

In this study, a condensation heat transfer experiment setup has been designed and constructed to carry out the condensation heat transfer study. The setup and experimental methods applied for this study is presented below.

3.1 Experimental setup design

A polymer plastic sheet is used to make a box with two chambers (one for cooling water and other one for steam) separated by vertical copper plate. Dimension of the box, cooling water chamber and steam chamber is $13 \times 11.5 \times 15 \text{ cm}^3$, $5.5 \times 11.5 \times 15 \text{ cm}^3$ and $7.5 \times 11.5 \times 15 \text{ cm}^3$ respectively. The polymer plastic sheet is cut at the required dimension and then assembled using araldite standard epoxy adhesive glue. Figure 3.1 shows the constructed experimental chamber used for the experiment.

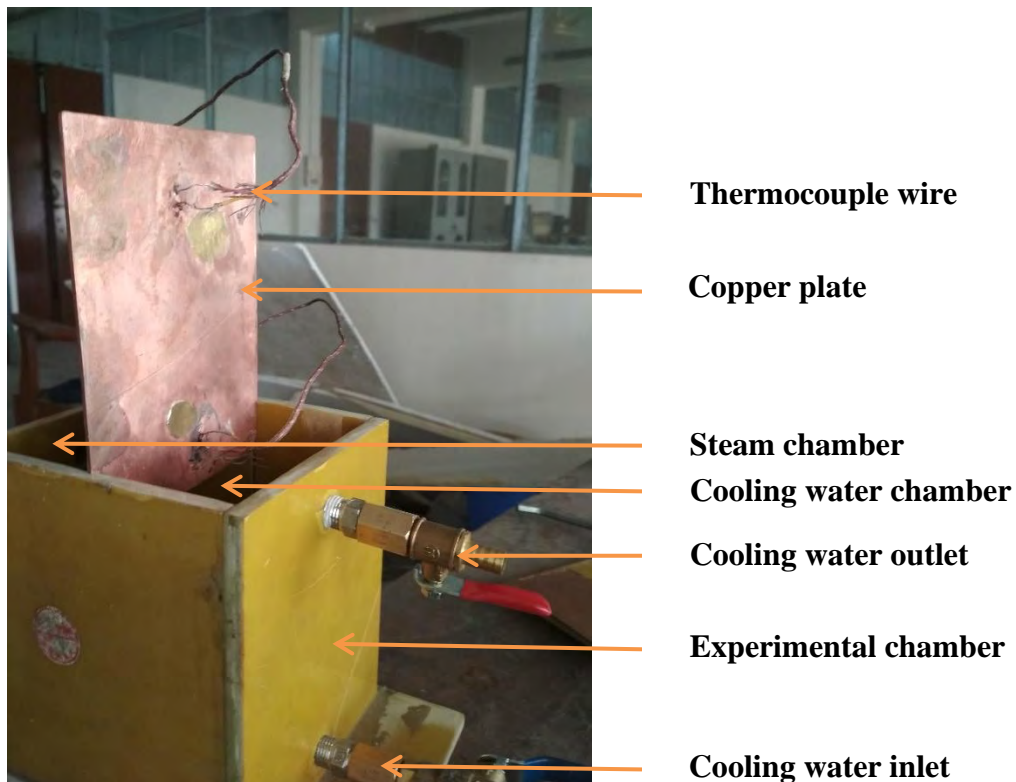


Figure 3.1: Constructed experiment chamber

Four copper surfaces (flat, rectangular shaped micro-grooved, sinusoidal shaped micro-grooved, and wedge shaped micro-grooved copper plate) of 150mm x 115mm x 2mm dimension are used as the condensing surface. The flat copper plate used for the experiment has been shown below in figure 3.2.

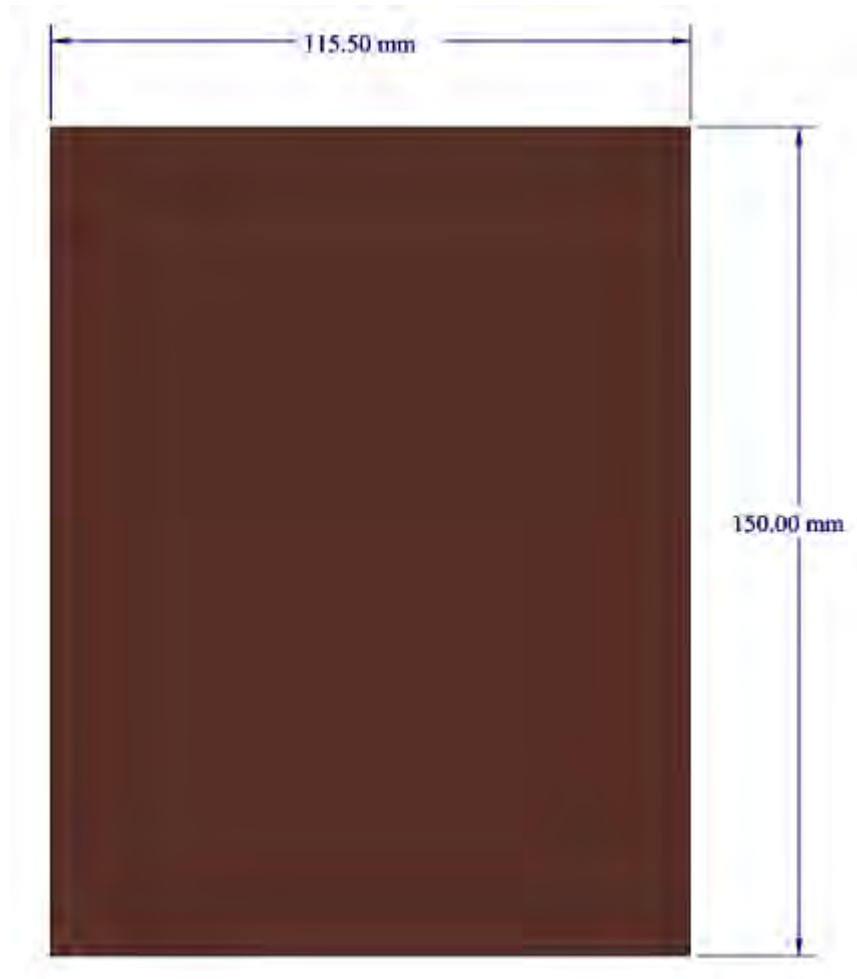


Figure 3.2: Flat copper plate

Rectangular shaped microgrooves having 700 x 500 μm dimension and 4.5mm spacing from each other are introduced along the longitudinal direction of the copper plate. The modified copper plate and the cross-sectional view of a single micro-groove has been shown in figure 3.3.

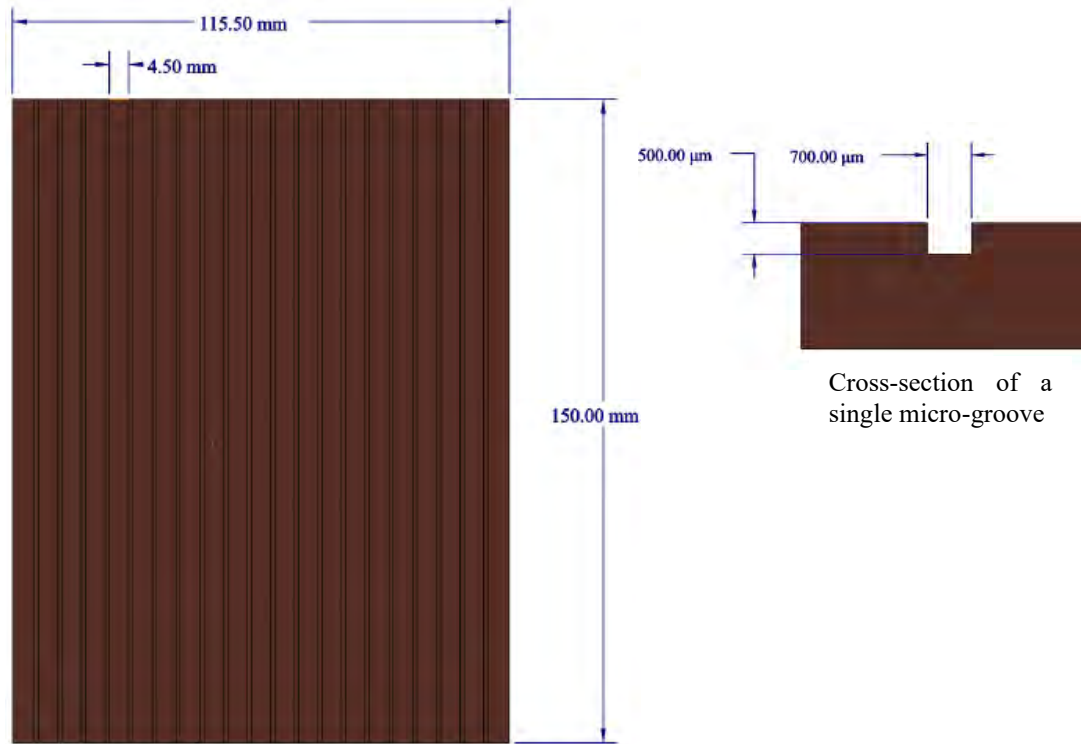


Figure 3.3: Rectangular shaped micro-grooved copper plate

Sinusoidal shaped microgrooves having $700 \times 500 \mu\text{m}$ dimension and 4mm spacing from each other are introduced along the longitudinal direction of the copper plate. Wavelength of constructed sinusoidal shaped micro-groove is 12mm and height of the wave is 3mm. Cross section of the micro-grooves are similar as in rectangular shaped micro-grooved copper plate. The modified copper plate and the cross-sectional view of a single micro-groove has been shown in figure 3.4.

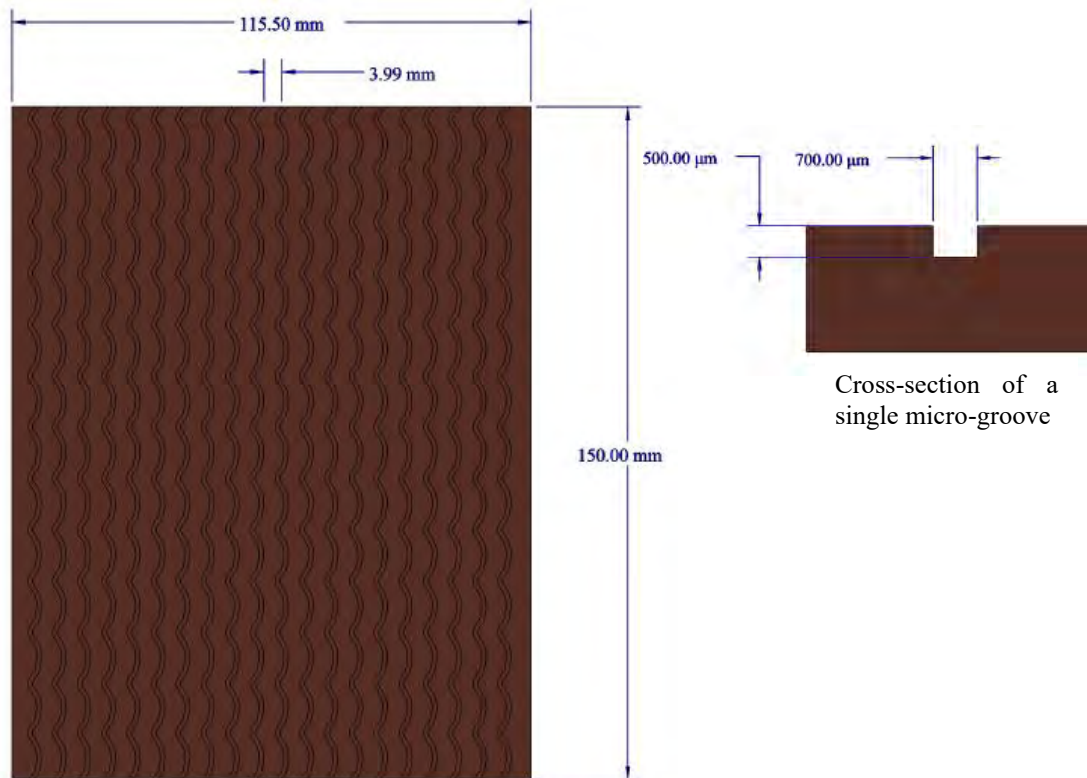


Figure 3.4: Sinusoidal shaped micro-grooved copper plate

All the micro-grooves (rectangular, sinusoidal and leaf vein shape) are introduced using pantograph mechanism. Pantograph instrument is used for duplicating a motion or copying a geometric shape to a reduced or enlarged scale. The pantograph engraving machine's operation principle is based on a four-bar system, with one link fixed and the others pivoting. These other links move in sync with the tracing link's movement. This is a low-cost but high-value device.

Finally, leaf vein shape structure (wedge shape) is tried to mimic on the flat copper plate. The dimension and cross section of microgrooves are similar as rectangular and sinusoidal shaped micro-grooved copper plate. The wedge shaped micro-grooved copper plate has been shown in figure 3.5.

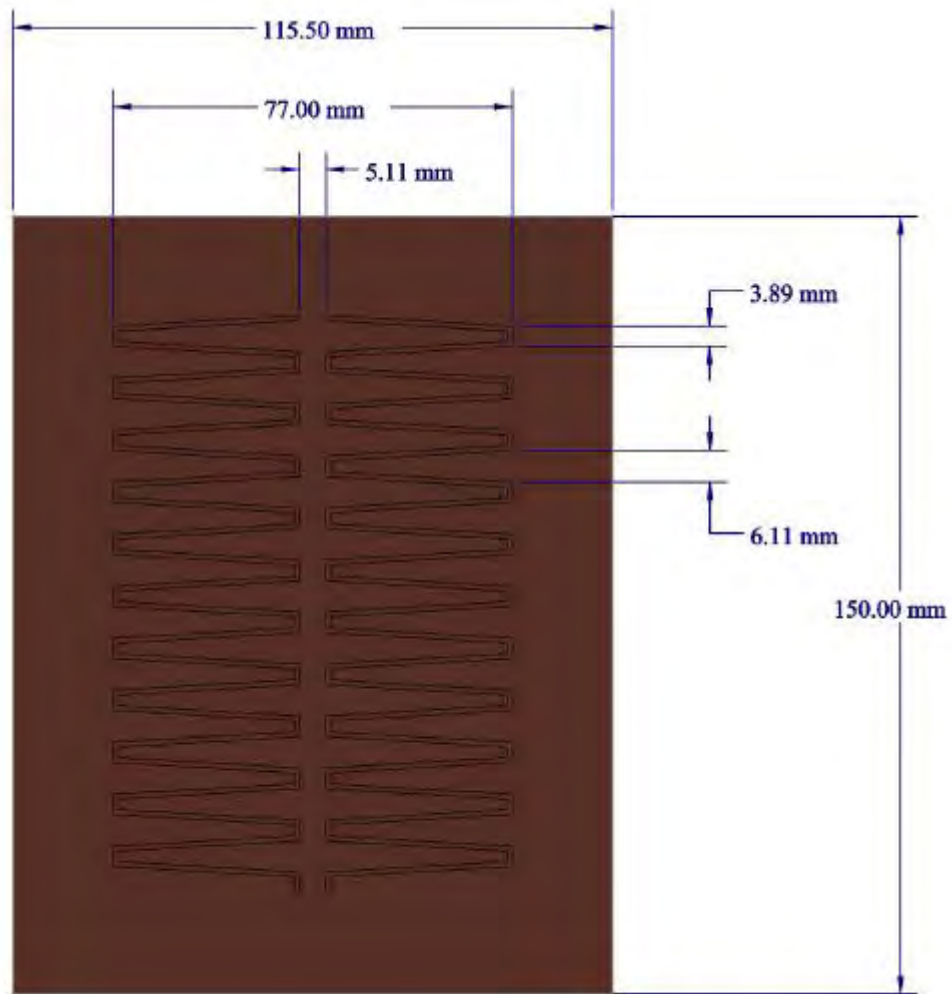


Figure 3.5: Wedge shaped micro-grooved copper plate

Two thermocouple wires are used at the upper and lower part of the plate to measure the surface temperature. The plate temperature was calculated by averaging temperature of the thermocouple. K-type (chromel-alumel) calibrated thermocouple was used in this experiment. Water temperature of the cooling water chamber was measured by a thermocouple inserting into the chamber. These thermocouple wires are directly connected to the pre-calibrated temperature meter via selector switch. To measure the inlet cooling water temperature a glass type thermometer was used in this experiment.

An externally fired; natural circulated; low pressure; vertical; 6L capacity mini boiler is constructed at the lab for this experiment to generate steam. A pressure gauge and a

temperature sensor are mounted on top of the boiler to measure pressure and temperature of the steam as shown in figure 3.6.

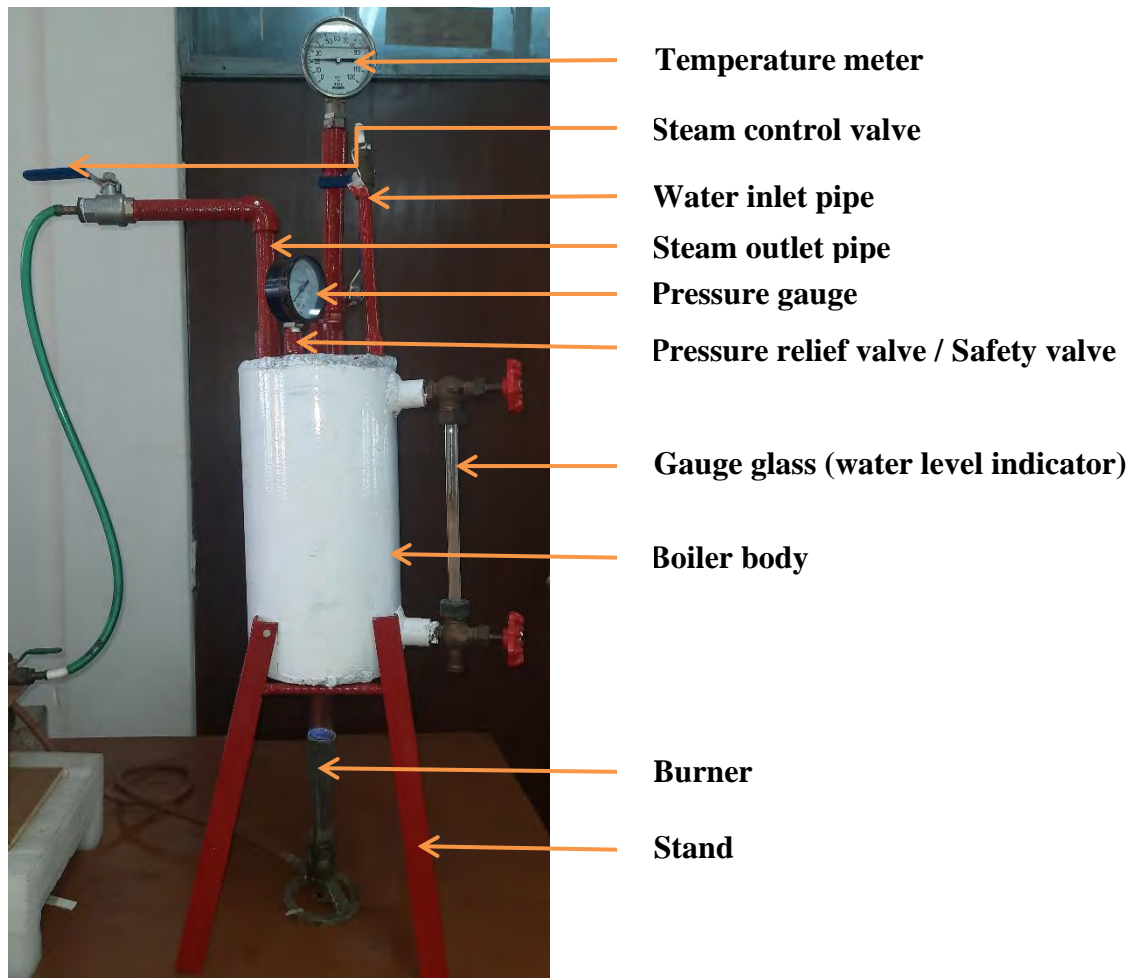


Figure 3.6: Constructed mini boiler

To know the level of water inside the boiler and to prevent the boiler from overheating a gauge glass is also attached with the boiler to act as water level indicator. Safety valve is inserted at the top of the boiler to save the boiler in case of pressure rise during steam generation. Steam was generated at just above the ambient pressure. Steam is fed into the steam chamber through the exhaust valve mounted at the top of the boiler. The whole boiler is supported by a triangular base and heat is supplied by a gas burner.

For cooling water circulation through the cooling water chamber a small submersible pump is used as shown in figure 3.7. Cooling water is flown from the bottom of the cooling water chamber to the top of the chamber against the gravity to maintain continuous contact of cooling water with the condensing surface. Flow rate of cooling

water is measured by stopwatch and bucket method [94]. Flow rate of water was controlled by ball valve.



Figure 3.7: Submersible pump

To record the surface morphological effect a camera has been used in this study. Configuration of the camera is advanced 24.2MP BSI full frame image sensor w/ 1.8X readout speed, 15 stop dynamic range, 14 bit uncompressed RAW, ISO 50 to 204,800, up to 10 fps silent or mechanical shutter with AE/AF tracking, Exmor R CMOS focus sensor.

3.1.1 Test loop

Before experiment all the part of the experimental setup were connected as presented in figure 3.8:

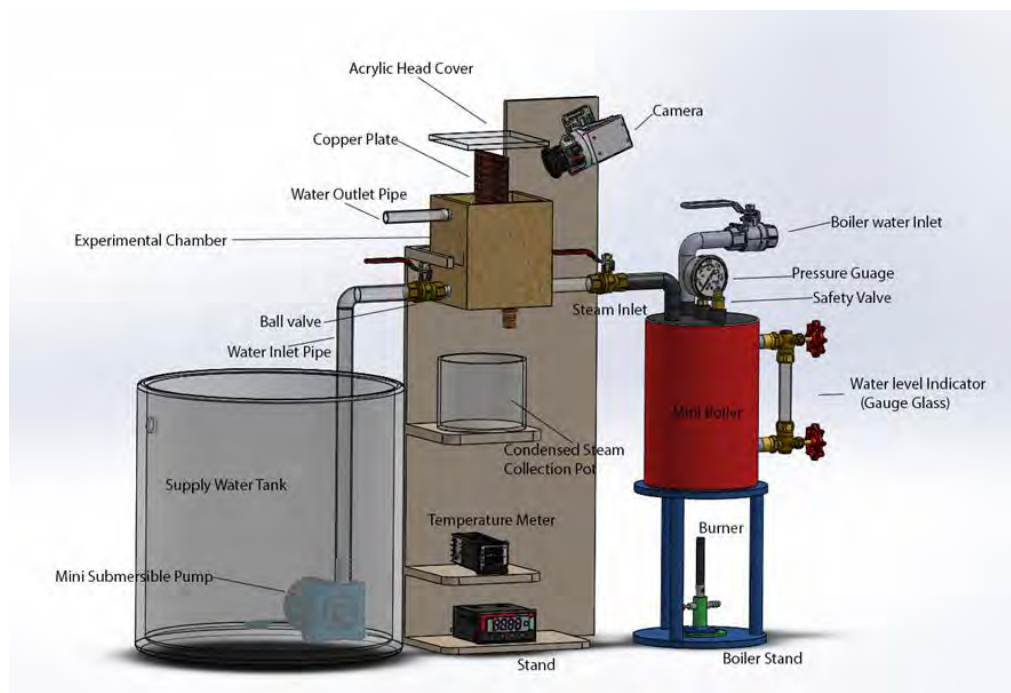


Figure 3.8: Experimental setup for the condensation heat transfer experiment

The loop is consisted of a steam generator, a test section, cooling water circulation and a drain. The entire flow loop was insulated to minimize heat loss. The top of the chamber is covered by a transparent acrylic sheet to monitor the droplet morphology parameters. Initially burner is kept on and temperature of boiler starts increasing, once the boiler reaches steady state condition and steam generates, the submersible pump was started. Flow rate of cooling water and steam is controlled by using two ball valves. Temperatures are recorded through temperature meter and thermometers throughout the experiment. Condensate is collected throughout the experiment and after the experiment condensate is weighed by a digital balance. A camera is used during the experiment to record the surface condensation morphology.

3.2 Data acquisition system

The most important part of an experiment is the collection of data. In the experiment, steam flow rate, cooling water flow rate, weight of the condensate, total experiment time and all necessary temperatures were measured once the system becomes stable after 1 hour.

3.2.1 Steam flow rate

Steam flow rate was not measured directly due to resource limitations, rather it was calculated from the weight of water inside the boiler and experiment running time. To ensure constant same flow rate, system pressure and heating condition was remain constant throughout the experiment.

3.2.2 Cooling water flow rate

Steam condensed on the copper plate by rejecting heat through the plate because the temperature of the plate is lower than the saturation temperature of the steam. The plate is cooled by the continuous contact of the cooling water supplied by the mini submersible pump. At the time of starting of the experiment a stopwatch is started to record the experimental time. Outlet water from cooling water chamber is collected in a bucket. The bucket is weighted by a digital balance whose resolution is one gram. Weight difference between bucket with water and empty bucket give the mass of water

collected in the experimental time. The mass of water dividing by the total time t gives the mass flow rate of cooling water.

3.2.3 Condensate drainage rate

Steam condenses on the experimental surfaces forming droplet on it and fall due to gravity. This condensate is collected in a pot. The weight difference between pot with condensate and empty pot give the total mass of condensate collected. Then the condensate collected divided by the experimental time gives the condensate drainage rate.

3.2.4 Temperature

In this experiment five different temperatures were measured. Two thermocouple wires are connected with experimental surfaces. One is on upper portion and another on lower portion of the plate. One thermocouple was inserted in the middle of cooling water chamber which give the temperature of water inside the cooling chamber. All the three thermocouple wires are connected to the digital temperature meter through a selector switch. During the experiment by rotating the nob of the selector switch the upper and lower plate temperature and the temperature of the cooling water inside the coolant chamber are taken. Then the temperature of inlet cooling water and outlet water from cooling chamber is also measured using thermometers. Steam temperature is measured by a temperature sensor mounted at the top of the boiler.

3.2.5 Time

By using a stopwatch, the total experimental time for a complete experimental process is measured.

3.3 Experimental process

As mentioned above, the complete experimental setup up is assembled and made ready to start the experiment. All the devices are connected as shown in figure 3.9. The steam is generated in the boiler. Water inside the boiler is measured before and after the experiment to find the amount of steam passed through the chamber. Water level inside the boiler can be known by a water level indicator mounted at the boiler. Finally, the

steam line is opened to supply the steam inside the condensation chamber. Simultaneously the submersible pump is started to circulate water inside the cooling water chamber.

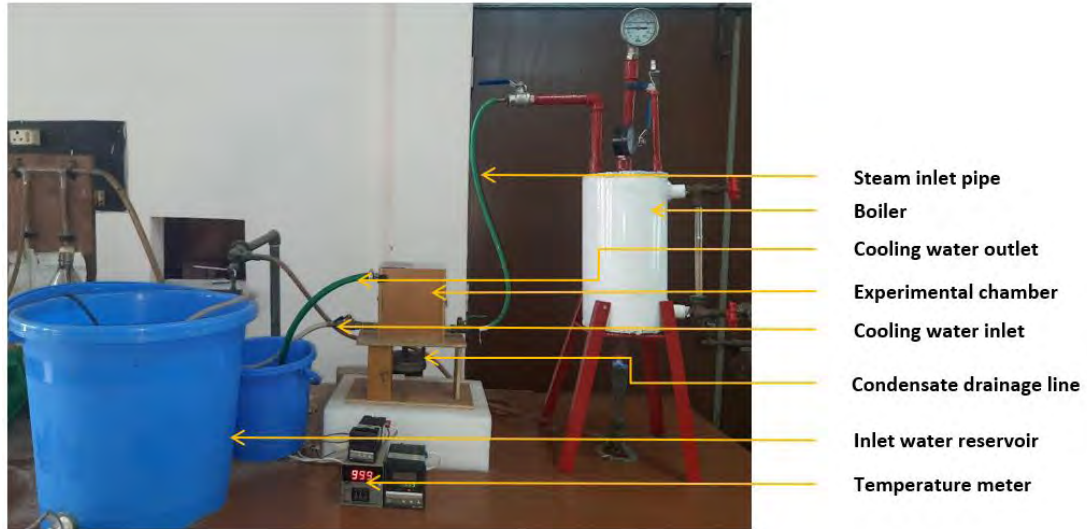


Figure 3.9: Actual photo of experimental setup

The cooling water flows through the chamber and it is collected from outlet. The condensation chamber enables vapor to flow freely and the heat transfer from vapor to condensation surface is spontaneous.

Steam is fed into the steam chamber for about 30 minutes to reach steady state condition. Once the system is in steady state condition, data was taken at 1 minute interval for 35 minutes. The whole process was repeated five times to ensure consistency and reliability of the experimental data.

3.4 Data analysis

In this study T_1 , T_2 , T_3 , T_4 , T_5 represents the upper surface temperature, cooling water outlet temperature, lower surface temperature, steam inlet temperature and cooling water inlet temperature respectively. Condensing surface temperature was determined by averaging the upper and lower surface temperature as shown below,

$$T_{\text{surf}} = \frac{T_1 + T_3}{2} \quad (3.1)$$

Heat flux q is calculated by,

$$q = \frac{\dot{m}_c C_p (T_2 - T_5)}{A} \quad (3.2)$$

Where \dot{m}_c , C_p , q and A denote the mass flow rate of cooling water, specific heat of cooling water at constant pressure, heat flux on condensing surface during condensation and effective condensation surface area (0.016m^2), respectively.

The calculation and heat transfer analysis of this study is based on Leu *et al.* [95]. Heat transfer Co-efficient can be calculated by,

$$h_c = \frac{q}{\Delta T} = \frac{q}{T_4 - T_{\text{surf}}} \quad (3.3)$$

Where h_c , q and ΔT denote the condensation heat transfer Co-efficient, heat flux on condensing surface during condensation and temperature difference between inlet steam and condensation surface, respectively.

Condensation surface temperature is calculated by:

$$q = -k_c \frac{dT}{dx} = -k_c \frac{T_1 - T_{\text{surf}}}{\Delta x} \quad (3.4)$$

$$T_1 + \frac{q\Delta x}{k_c} = T_{\text{surf}} \quad (3.5)$$

Where K_c and Δx denote the thermal conductivity of copper and distance between thermocouple and condensation surface, respectively. This equation represents one dimensional thermal conduction mode of Fourier's heat conduction law.

3.5 Uncertainty analysis

In any experiment uncertainties are caused by factors such as limitations of the instrument and random fluctuations in the test environment. As the experiment involves multiple measurements such as temperature, mass of water and condensate, time, mass of empty bucket, empty boiler, dimension of the flat plate, etc. The uncertainty of each measurement contribute to the result.

Two types of error can occur, one is systematic error and the other one is measuring error. The systematic error occurs usually by un-calibrated or mis-calibrated instrument. The measuring error can occur for relative mis-observation or measuring values larger or smaller than it actually is. For single measurement the uncertainty is a fixed number. But this particular value can vary considering the particular circumstances of observation.

Uncertainties in Measurands:

a. Precision limit, P: This is an estimate of the lack of repeatability caused by random errors and process unsteadiness. This element can be sampled with the available procedure and apparatus should be based on statistical estimates from samples whenever possible.

b. Bias limit, B: The bias limit is an estimate of the magnitude of the fixed constant error. This element cannot be sampled within available procedure and its existence is what mandates the need of cross-checks.

c. Uncertainty, W: The ± 5 interval about the nominal results is the band within which the experiment is 95% confident that the true value of the result lies. And it is calculated from the following:

$$W = (P^2 + B^2)^{\frac{1}{2}} \tag{3.6}$$

In the experiment the uncertainty associated with the measurement was estimated as

Table 1: Bias limit of measurands

Measurand	Bias limit	Value of Bias limit
Mass	B_m	0.0005 kg
Temperature	B_T	0.5 °C
Dimension	B_H, B_W	0.005 mm
Time	B_t	0.05 s

For calculating heat flux the conventional heat transfer equation is used that can also be written in the following form:

$$q = \frac{mc_p(T_2 - T_5)}{H \times W \times t} \quad (3.7)$$

$$\dot{m} = \frac{m}{t} = \text{mass flow rate in kg/s}$$

$A = H \times W =$ Effective condensation heat transfer area

Here, H and W represent height and width of the flat copper plate.

The uncertainty of heat flux is represented by the following equation:

$$w_q = \left[\left(\frac{\partial q}{\partial m} w_m \right)^2 + \left(\frac{\partial q}{\partial T_5} w_{T_5} \right)^2 + \left(\frac{\partial q}{\partial T_2} w_{T_2} \right)^2 + \left(\frac{\partial q}{\partial H} w_H \right)^2 + \left(\frac{\partial q}{\partial W} w_W \right)^2 + \left(\frac{\partial q}{\partial t} w_t \right)^2 \right]^{1/2} \quad (3.8)$$

The condensation heat transfer coefficient is calculated by using the following formula:

$$h_c = \frac{q}{\Delta T} = \frac{q}{T_4 - T_{\text{surf}}} = \frac{2q}{2T_4 - T_1 - T_3} \quad (3.9)$$

The uncertainty in condensation heat transfer coefficient is calculated by using the following formula:

$$w_{h_c} = \left[\left(\frac{\partial h_c}{\partial q} w_q \right)^2 + \left(\frac{\partial h_c}{\partial T_1} w_{T_1} \right)^2 + \left(\frac{\partial h_c}{\partial T_3} w_{T_3} \right)^2 + \left(\frac{\partial h_c}{\partial T_4} w_{T_4} \right)^2 \right]^{1/2} \quad (3.10)$$

Similar formulae are used to calculate the uncertainty in heat flux and condensation heat transfer coefficient for the modified copper plates. A sample calculation of uncertainty analysis has been shown in Appendix 6.

The maximum uncertainty associated with different parameters are calculated as presented below.

Table 2: Uncertainty in estimated parameters

Estimated parameter		Uncertainty (%)
Heat flux	Flat plate	± 8.32
	Wedge shape	± 8.27
	Sine shape	± 8.29
	Rectangular shape	± 8.26
Heat transfer coefficient	Flat plate	± 8.33
	Wedge shape	± 8.27
	Sine shape	± 8.29
	Rectangular shape	± 8.26

From the value of maximum uncertainty associated with different parameters it can be said that the experimental results are reliable.

CHAPTER 4: EXPERIMENTAL RESULTS AND DISCUSSION

Surface wettability, droplet morphological parameters such as droplet size, droplet frequency, droplet growth rate, droplet coalescence rate, droplet drainage rate along with the heat transfer behavior of flat and modified copper plates has been studied. A comparative analysis among these surfaces has also been performed here.

4.1 Study on surface wettability

Figure 4.1 shows the wetting behavior of the copper surfaces studied for the experiments. The contact angle is determined by looking at the droplet profile and measuring the angle directly. The contact angle of a water droplet on a flat copper plate is measured as 90 degrees, for the wedge shaped micro-grooved copper plate it is 103 degrees, for the sinusoidal shaped micro-grooved copper plate it is 114 degrees, and it is 122 degrees for the rectangular micro-grooved copper plate.



(a) On flat copper plate

$$\theta = 89.7^\circ$$



(b) On wedge shaped micro-grooved copper plate

$$\theta = 103.3^\circ$$



(c) On sinusoidal shaped micro-grooved copper plate

$$\theta = 113.8^\circ$$



(d) On rectangular shaped micro-grooved copper plate

$$\theta = 121.7^\circ$$

Figure 4.1: Contact angle of droplets on flat and micro-grooved copper plate

Low contact angle values indicate that the liquid wets the surface, whereas high contact angle values suggest that the liquid spreads poorly. When the contact angle is less than 90 degrees, the liquid is said to soak the surface. In comparison to flat copper plate, wedge shaped micro-grooved copper plate, sinusoidal shaped micro-grooved copper plate and rectangular micro-grooved copper plate possesses a significant increase in contact angle. As a result, flat copper plate is more wettable than other micro grooved copper plates, similar findings also have been reported by Chau *et. al* [52], implying that dropwise condensation on micro-grooved copper surfaces are more sustainable than dropwise condensation on flat copper plate.

4.2 Surface condensation morphology

This research also investigates surface condensation analysis. Droplet formation, droplet growth, droplet coalescence, droplet departure, and other characteristics have been recorded by a camera. The surface condensation morphology on the experimental copper surfaces has been discussed below.

4.2.1 Condensation morphology on flat copper plate

The droplet condensation behavior of flat copper plate has been shown presented in figure 4.2. The time shown underneath each image indicates experiment's operation time at the moment it was captured. At $t = 3s$, dropwise condensation mode of heat transfer appeared first. A large number of droplets of various sizes generated from the active nucleation sites and the droplet grows with time $t = 7s$. At $t = 11s$, droplets are coalescing with adjacent droplets along its falling path and starts shedding from the condensing surface due to gravity at $t = 18s$. The surface rejuvenation process is continued. At $t = 14 \text{ min}$, a film like droplet is appeared as shown in figure 4.2 (b) which became enlarged with time and finally departed from the surface as shown in figure 4.2. At $t = 30 \text{ min}$, film like membrane is appeared and it covered a significant portion of the condensing surface. The striking velocity of steam jet on condensing surface was 0.03 m/s and from the record captured by the camera it is also obvious that the steam jet velocity has very negligible effect here. That's why steam jet velocity effect has not been considered in any of the cases.

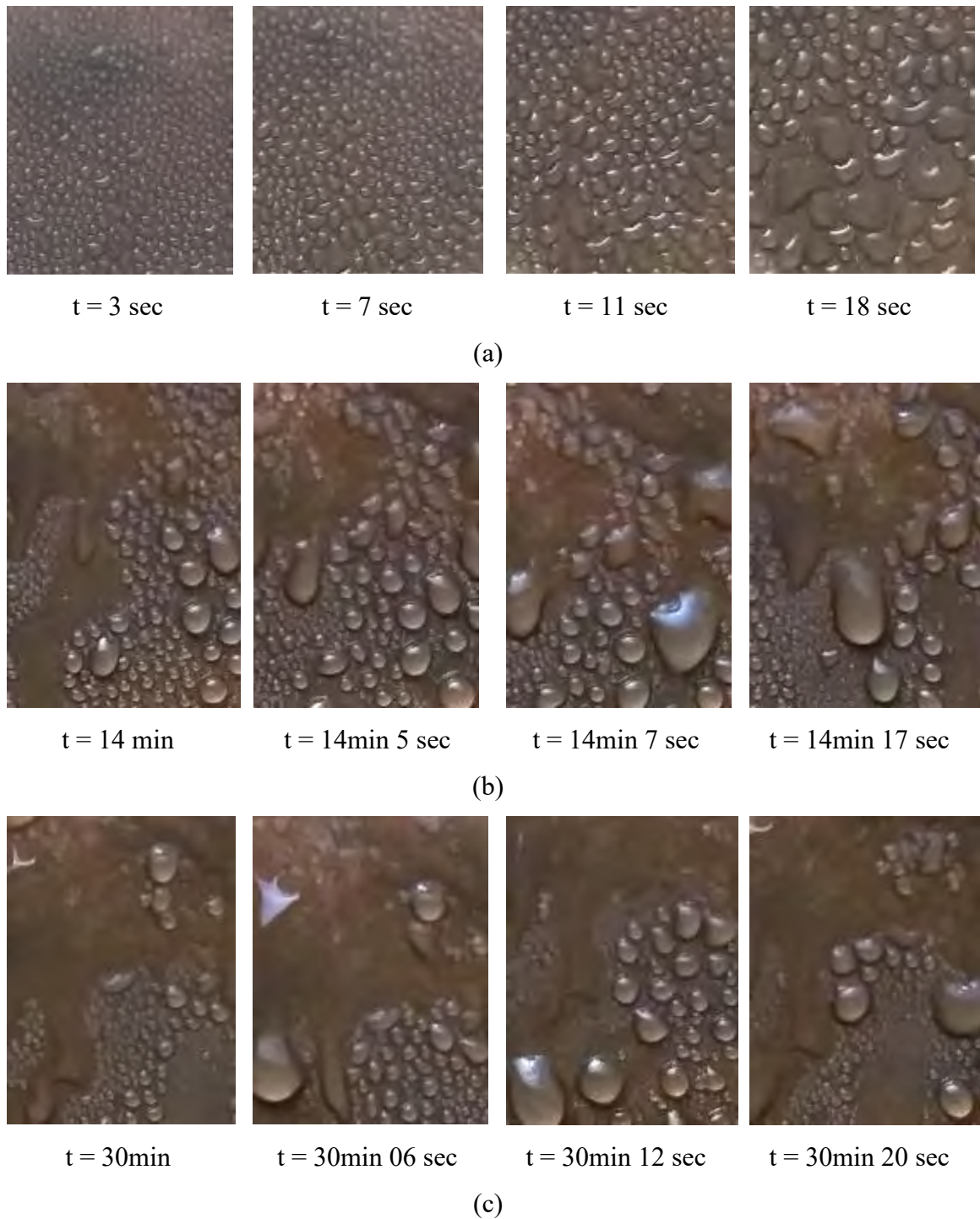


Figure 4.2: Condensation morphology on flat copper plate (3x magnification)

4.2.2 Condensation morphology on wedge shaped micro grooved copper plate

Droplet condensation morphology on wedge shaped micro-grooved copper plate has been shown in figure 4.3.

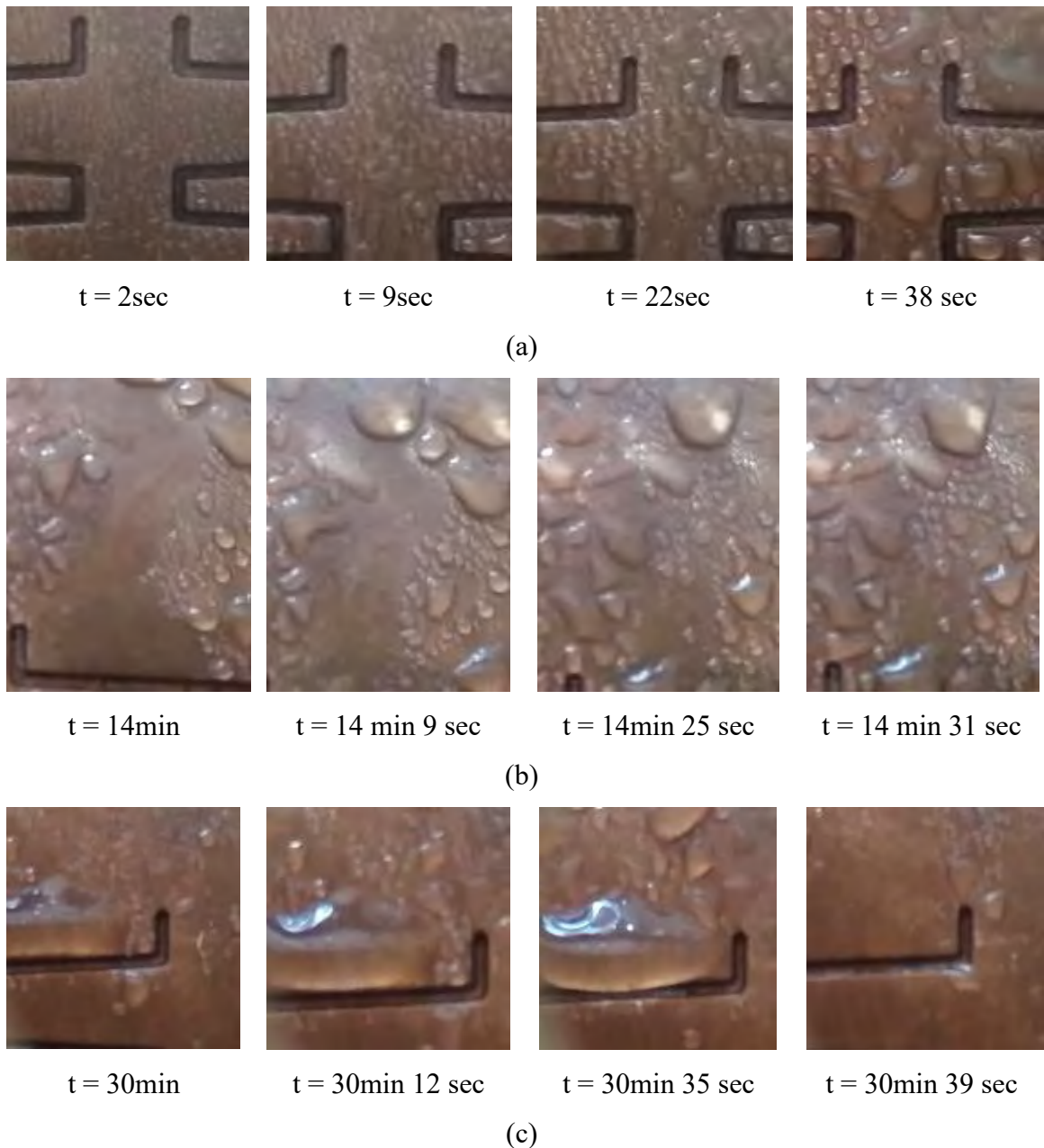


Figure 4.3: Condensation morphology on wedge shaped micro-grooved copper plate (3x magnification)

Droplet generation from nucleation sites has been shown at $t = 2\text{ s}$ in figure 4.3 (a). Dropwise condensation is visible on the condensing surface and many spherical droplets of varying sizes appeared. The droplet grows and coalesce with time as shown at $t = 9\text{ s}$ and $t = 22\text{ s}$ respectively. Finally, at $t = 38\text{ s}$, droplets shed by gravity falls from the condensing surface. At $t = 14\text{ min}$, thin liquid film along with large droplets appeared on the condensing surface and the droplets are coalescing along their falling

path and finally departed from the condensing surface. At $t = 30\text{min}$, very large droplets are appeared adjacent to micro-grooves. Until $t = 30\text{min } 35\text{ sec}$ the droplet is getting large by coalescing with adjacent droplets and finally at $t = 30\text{ min } 39\text{ sec}$ new surface rejuvenation process starts. Here, it is noticed that falling droplets are taking time to fall from the condensing surface due to the energy barrier created by the horizontal groove lines. The falling droplets only fall from the surface when it is at a certain size to overcome the energy barrier.

From the comparative analysis of droplet morphology on flat copper plate and wedge shaped micro-grooved copper plate, it is observed from figure 4.2 and figure 4.3 that flat copper plate possesses higher nucleation density compared to wedge shaped micro-grooved copper plate which matches well with the results obtained by Attinger *et al.* [42] and this is one of the main reasons for film like droplet appearance at flat copper plate. Heat transfer Co-efficient is inversely proportional to nucleation density. So, higher heat transfer Co-efficient is expected for wedge shaped micro-grooved copper plate compared to flat copper plate. From the droplet morphology analysis, it is also observed that departed droplet diameter has been 24% increased approximately in case of wedge shaped micro-grooved copper plate compared to flat copper plate. The condensate drainage rate was found to be 5% lower for wedge shaped micro-grooved copper plate compared to that of flat copper plate. It is due to the increment of departed droplets diameter and rejuvenation time in case of wedge shaped micro-grooved copper plate compared to that of flat copper plate.

4.2.3 Condensation morphology on sinusoidal shaped micro grooved copper plate

Droplet condensation morphology on sinusoidal shaped micro-grooved copper plate has been shown in figure 4.4. From figure 4.4 (a), at $t = 5\text{s}$, droplet generation from active nucleation sites has been shown. Dropwise condensation is visible on the condensing surface and many spherical droplets of varying sizes appeared. Then droplet growth and coalescing have been shown at $t = 9\text{s}$ and $t = 15\text{s}$ respectively. Finally, at $t = 25\text{s}$, droplets shed by gravity fall from the condensing surface. Here an interesting phenomenon is observed that is the falling droplets follow the path between two parallel micro-grooves not in a scattered path like condensation on flat plate. The

departed droplets follow slightly jig jag path not perfectly straight path like in rectangular micro-grooved copper plate. At $t = 14\text{min}$, large droplets appeared on the condensing surface then the droplets are coalescing along their falling path and finally departed from the surface. Finally, at $t = 30\text{min}$, thin film membrane is appeared. Here droplet generation is decreased due to formation of film like membrane.

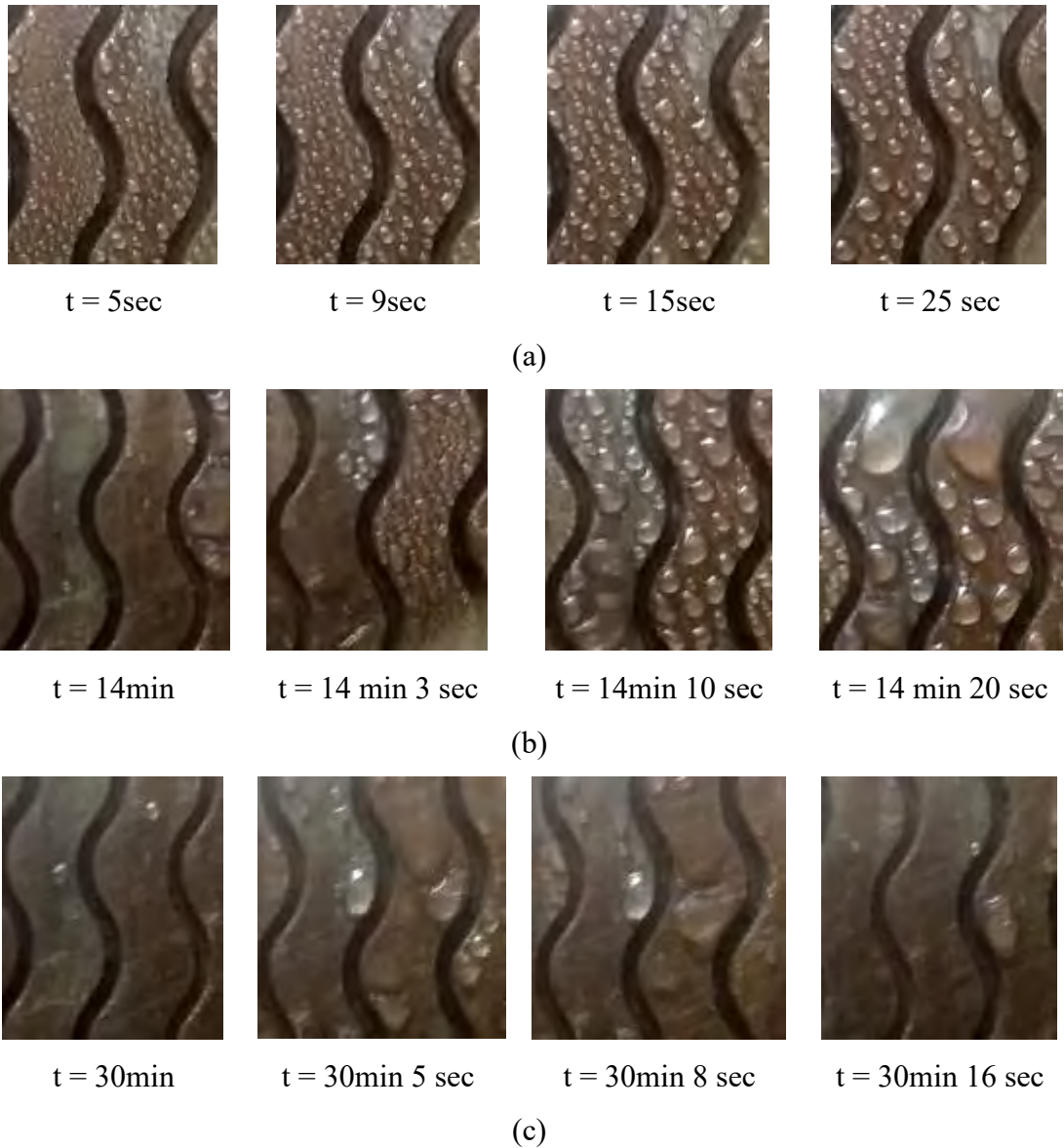


Figure 4.4: Condensation morphology on sinusoidal shaped micro-grooved copper plate (3x magnification)

From the comparative analysis of droplet morphology on flat copper plate and sinusoidal shaped micro-grooved copper plate, it is observed from figure 4.2 and figure

4.4 that flat copper plate possesses higher nucleation density compared to sinusoidal shaped micro-grooved copper plate and this is one of the main reasons for film like droplet appearance at flat copper plate at an earlier stage. From the droplet morphology analysis, it is also observed that departed droplet diameter has been 27% decreased approximately in case of sinusoidal shaped micro-grooved copper plate compared to flat copper plate. Heat transfer Co-efficient is inversely proportional to droplet size. So, higher heat transfer Co-efficient is expected for sinusoidal shaped micro-grooved copper plate compared to flat copper plate. The condensate drainage rate was found to be 9% higher for sinusoidal shaped micro-grooved copper plate compared to that of flat copper plate. It is due to the increment of sliding velocity of falling droplets of sinusoidal shaped micro-grooved copper plate compared to that of flat copper plate.

4.2.4 Condensation morphology on rectangular shaped micro-grooved copper plate

Droplet condensation morphology on rectangular micro-grooved copper plate has been shown in figure 4.5. From figure 4.5 (a), at $t = 5s$, droplet generation from active nucleation sites has been shown. Dropwise condensation is visible on the condensing surface and many spherical droplets of varying sizes appeared. Then droplet growth and coalescing have been shown at $t = 9s$ and $t = 15s$ respectively. Finally, at $t = 25s$, droplets shed by gravity fall from the condensing surface. Here an interesting phenomenon is observed that is the falling droplets follow the path between two parallel micro-grooves not in a scattered path like condensation on flat plate. At $t = 14min$, large droplets appeared on the condensing surface then the droplets are coalescing along their falling path and finally departed from the surface. Finally, at $t = 30min$, film like membrane is appeared and finally the droplets departed from the surface. Here droplet generation is decreased due to formation of film like membrane. Now, it is noticeable from the condensation morphology on the flat and modified surfaces that droplet embryos are postulated to form and grow at the nucleation sites, while portions of the surface between the growing droplets remain dry which is actually the first model of dropwise condensation [88] and this model matches well with the obtained experimental results.

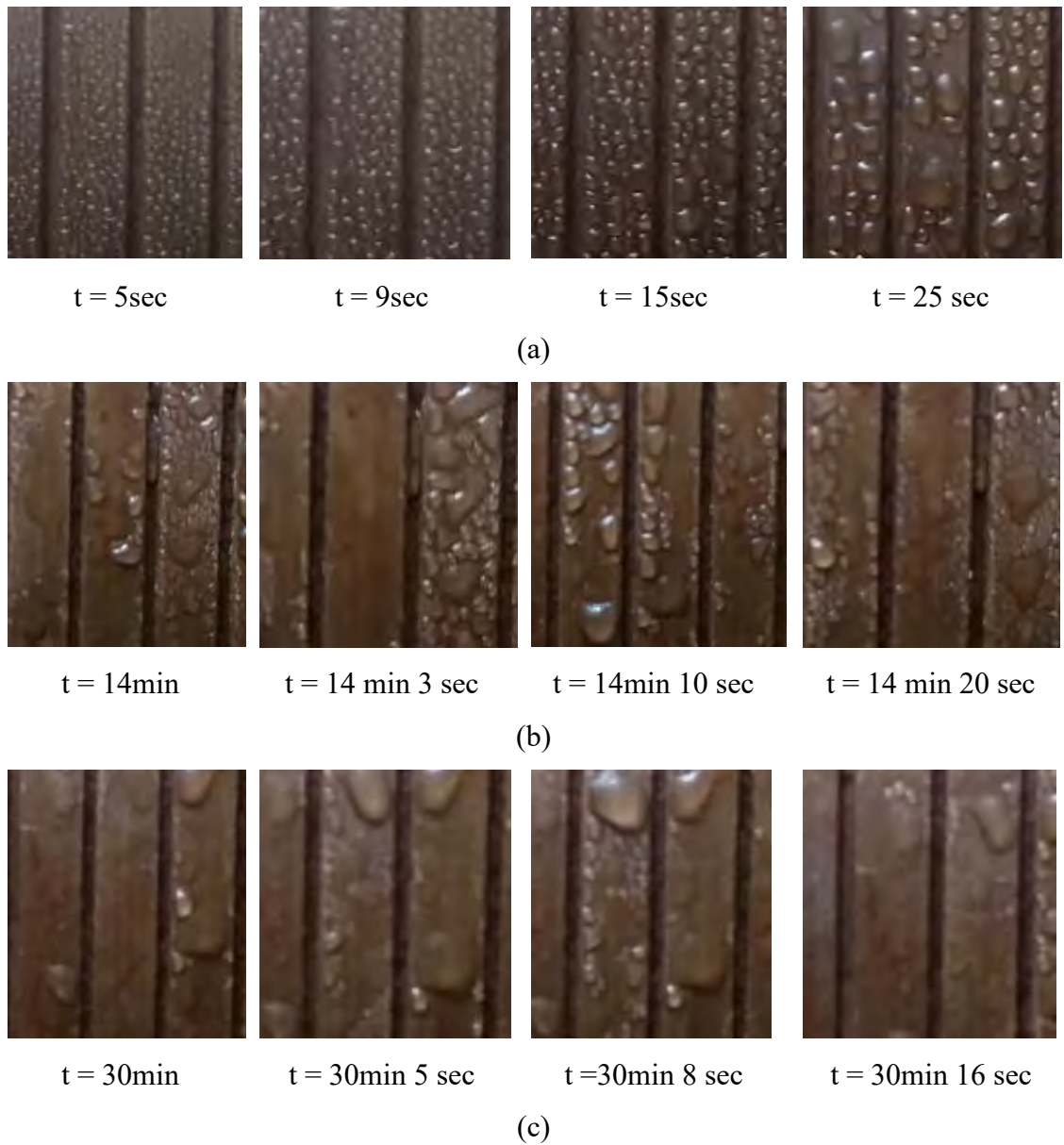


Figure 4.5: Condensation morphology on rectangular micro-grooved copper plate (3x magnification)

From the comparative analysis of droplet morphology on flat copper plate and rectangular micro-grooved copper plate, it is observed from figure 4.2 and figure 4.5 that flat copper plate possesses higher nucleation density compared to rectangular micro-grooved copper plate and this is one of the main reasons for film like droplet appearance at flat copper plate at an earlier stage. From the droplet morphology analysis, it is also observed that departed droplet diameter has been 33% decreased approximately in case of rectangular micro-grooved copper plate compared to flat copper plate. Heat transfer Co-efficient is inversely proportional to droplet size. So,

higher heat transfer Co-efficient is expected for rectangular shaped micro-grooved copper plate compared to flat copper plate. The condensate drainage rate was found to be 11.76% higher for rectangular shaped micro-grooved copper plate compared to that of flat copper plate. It is due to the increment of sliding velocity of falling droplets of rectangular micro-grooved copper plate compared to that of flat copper plate.

4.3 Heat transfer analysis

Heat transfer Co-efficient h_c has also been analyzed in this study. The heat transfer Co-efficient of micro-grooved copper surfaces is distinctly higher than that of flat copper plate for the same Sub-cooling temperature.

4.3.1 Effect of Sub-cooling temperature on heat transfer Co-efficient for flat copper plate

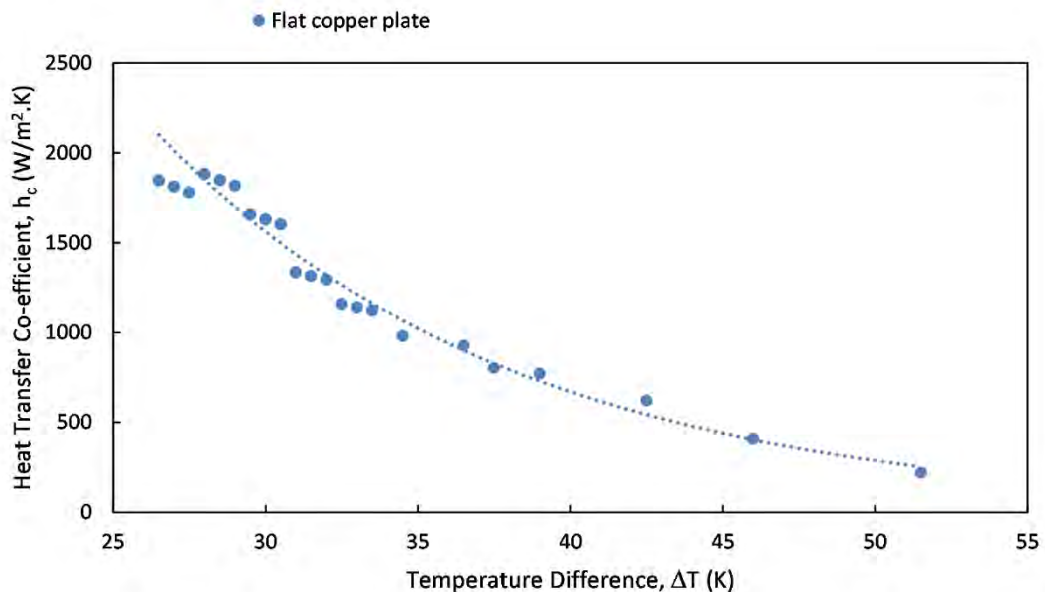


Figure 4.6: Variation of heat transfer Co-efficient with temperature difference for flat copper plate

Figure 4.6 shows the relationship between the heat transfer Co-efficient h_c and the temperature difference ΔT for flat copper plate. As the heat transfer Co-efficient is inversely proportional to the Sub-cooling temperature difference, the heat transfer Co-efficient decreases as the Sub-cooling temperature difference increases as shown in figure 4.6.

4.3.2 Effect of Sub-cooling temperature on heat transfer Co-efficient for wedge shaped micro grooved copper plate

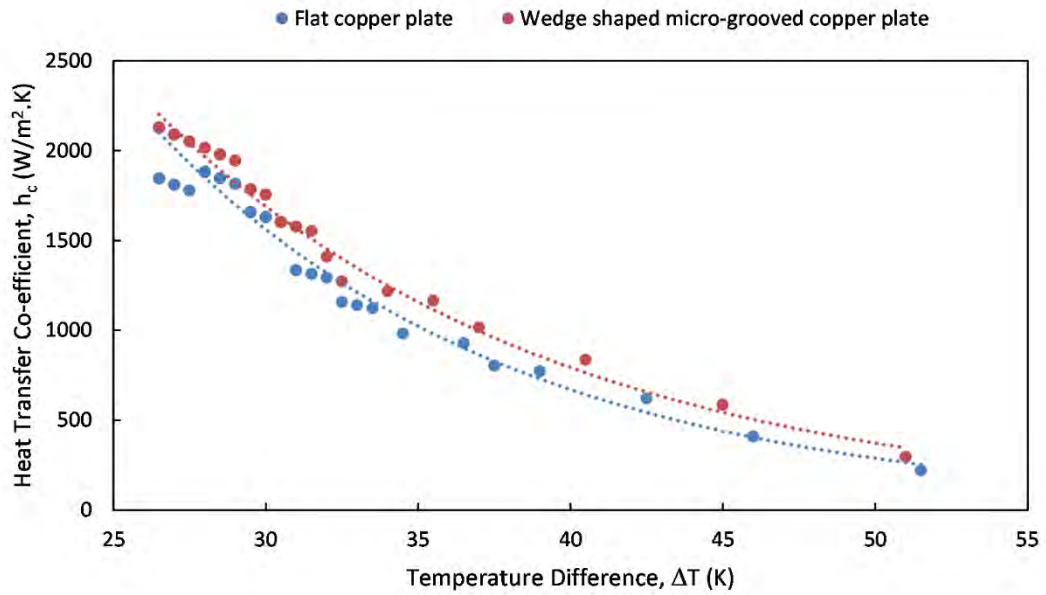


Figure 4.7: Variation of heat transfer Co-efficient with temperature difference for both flat and wedge shaped micro-grooved copper plate

Figure 4.7 shows the relationship between the heat transfer Co-efficient h_c and the temperature difference ΔT for both flat and wedge shaped micro-grooved copper plate. It is observed from figure 4.7 that the heat transfer Co-efficient of wedge shaped micro-grooved copper plate is 15-18% larger than flat plate at the same Sub-cooling temperature. This is due to the increment of contact angle for wedge shaped micro-grooved copper plate. Increment of contact angle makes the modified surface less wettable compared to flat copper plate. The heat transfer Co-efficient is also higher due to the relatively less nucleation density in wedge shaped micro-grooved copper plate compared to flat copper plate.

4.3.3 Effect of Sub-cooling temperature on heat transfer Co-efficient for sinusoidal shaped micro-grooved copper plate

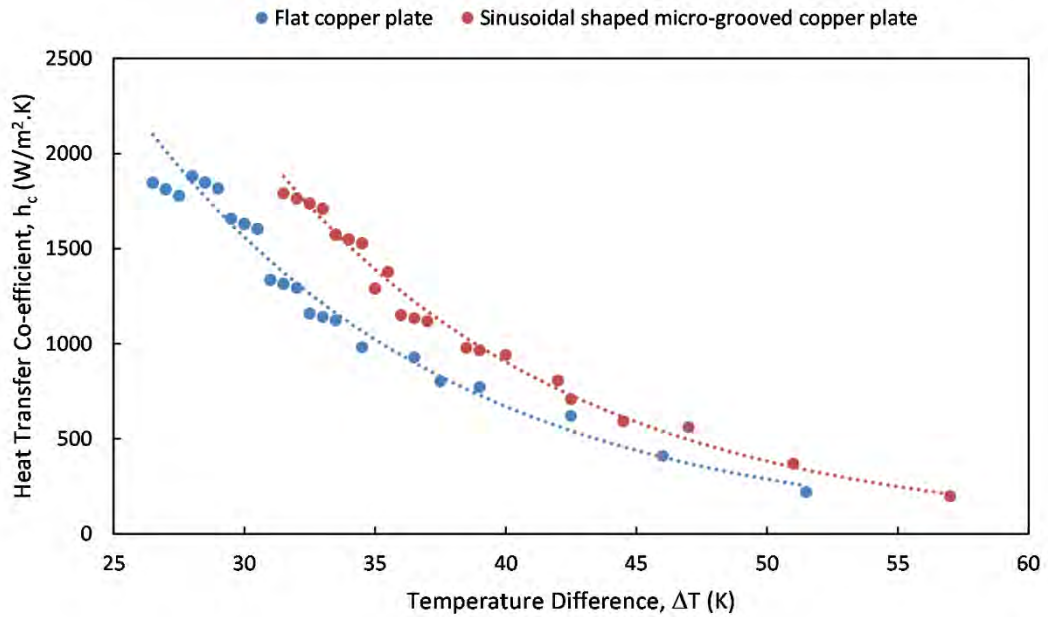


Figure 4.8: Variation of heat transfer Co-efficient with temperature difference for both flat and sinusoidal shaped micro-grooved copper plate

Figure 4.8 depicts the relationship between the heat transfer coefficient h_c and the temperature difference ΔT for both flat and sinusoidal shaped micro-grooved copper plate. As can be seen from figure 4.8 that at the same subcooling temperature, the heat transfer coefficient of a sinusoidal shaped micro-grooved copper plate is 15-50% higher than that of a flat plate. Increment of contact angle which makes the modified surface less wettable for sinusoidal shaped micro-grooved copper plate causes this increment in heat transfer Co-efficient. Due to the lower nucleation density in sinusoidal shaped micro-grooved copper plate compared to flat copper plate, the heat transfer Co-efficient is also higher. Also, the decrement of departed droplet diameter results in higher condensation heat transfer Co-efficient [20, 42] in case of sinusoidal shaped micro-grooved copper plate and this matches well with the existing work done by Tanasawa *et al.* [20].

4.3.4 Effect of Sub-cooling temperature on heat transfer Co-efficient for rectangular shaped micro-grooved copper plate

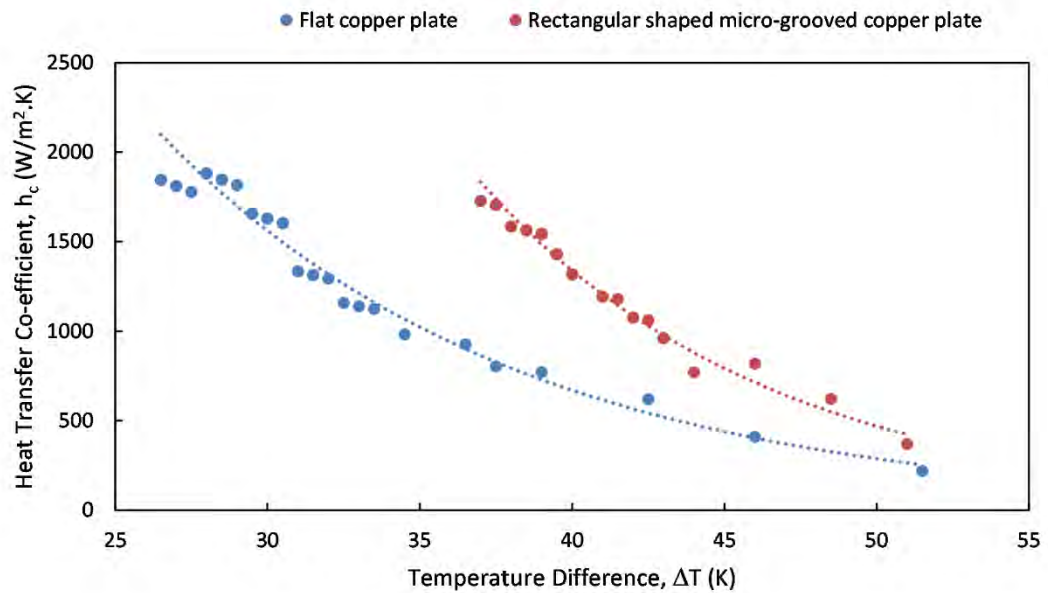


Figure 4.9: Variation of heat transfer Co-efficient with temperature difference for both flat and rectangular shaped micro-grooved copper plate

Figure 4.9 shows the relationship between the heat transfer Co-efficient h_c and the temperature difference ΔT for both flat and rectangular shaped micro-grooved copper plate. It is obvious that the rectangular micro-grooved copper plate has a significantly higher heat transfer coefficient than flat copper plate. It is observed from figure 4.9 that the heat transfer Co-efficient of rectangular micro-grooved copper plate is 20-60% higher than flat plate at same Sub-cooling temperature. This is due to the increment of contact angle for rectangular shaped micro-grooved copper plate. Increment of contact angle makes the modified surface less wettable compared to flat copper plate. Due to the lower nucleation density in rectangular shaped micro-grooved copper plate compared to flat copper plate, the heat transfer Co-efficient is also higher. In the case of rectangular shaped micro-grooved copper plate, the reduction with departing droplet diameter also results in a higher condensation heat transfer Co-efficient [20, 42].

4.3.5 Comparative analysis of effect of Sub-cooling temperature on heat transfer Co-efficient of flat and modified copper surfaces

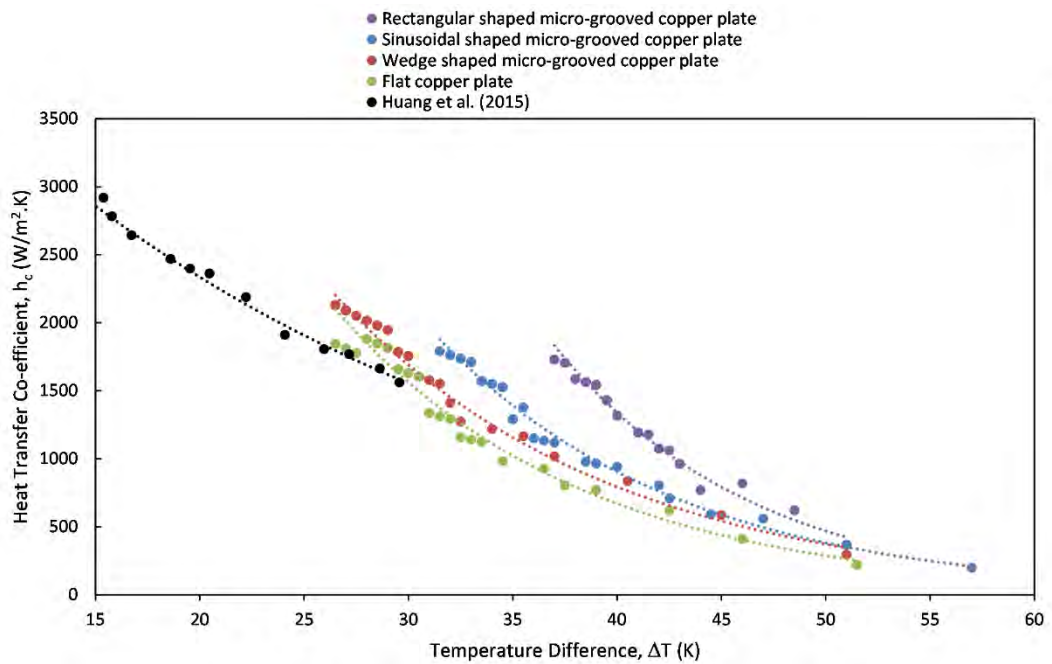


Figure 4.10: Variation of heat transfer Co-efficient with temperature difference for both flat and modified copper surfaces

Figure 4.10 shows a comparative analysis of heat transfer Co-efficient at different sub-cooling temperature difference for both flat and modified copper surfaces. Heat transfer Co-efficient is stably decreasing with increasing ΔT . The trend of the relationship between heat transfer Co-efficient and ΔT is similar to the results obtained by Huang *et al.* [96] on superhydrophobic surfaces. It is obvious from figure 4.10 that the condensation heat transfer Co-efficient of the modified copper surfaces is distinctly higher than that of the flat copper plate. The comparative analysis shows that the rectangular micro-grooved copper plate is less wettable and has the lowest diameter droplets among other experimental surfaces which causes the highest heat transfer Co-efficient at same sub-cooling temperature difference among other modified surfaces.

4.3.6 Effect of time on heat transfer Co-efficient for flat copper plate

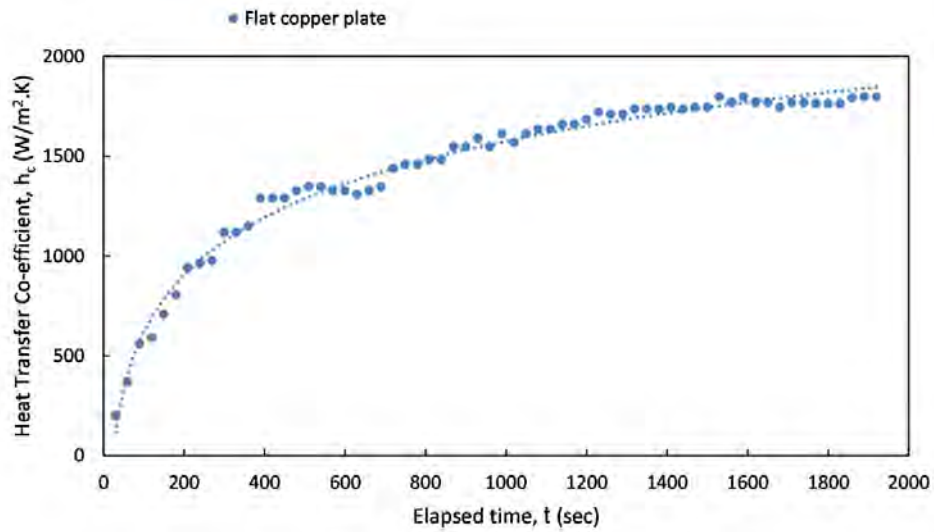


Figure 4.11: Variation of heat transfer Co-efficient with time for flat copper plate

Figure 4.11 shows the variation of heat transfer Co-efficient at different operation time of the experiment for flat copper plate. With the increment of time the sub-cooling temperature decreases and due to this reason heat transfer Co-efficient increases with operational time as it is inversely proportional to the sub-cooling temperature.

4.3.7 Effect of time on heat transfer Co-efficient for wedge shaped micro-grooved copper plate

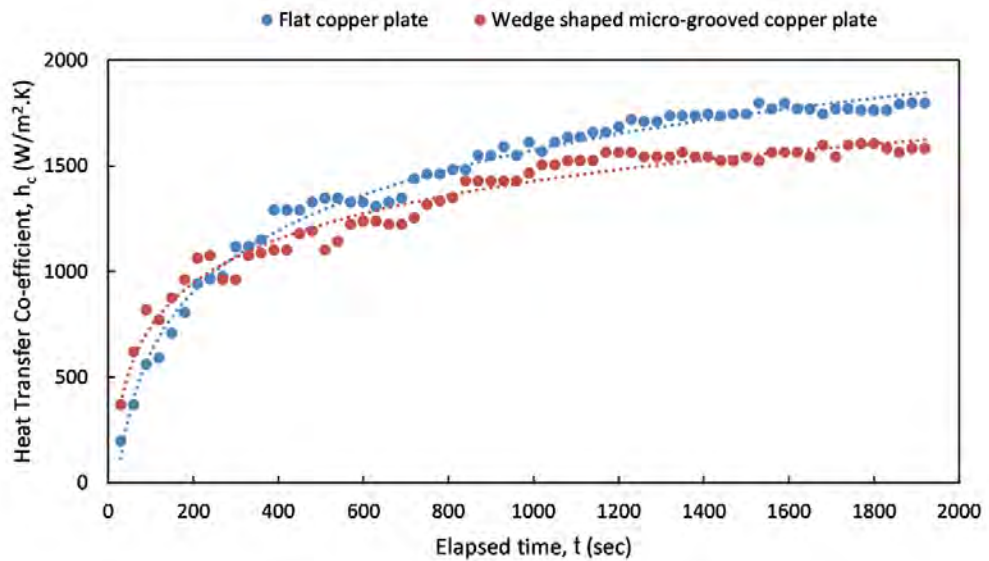


Figure 4.12: Variation of heat transfer Co-efficient with time for both flat and wedge shaped micro-grooved copper plate

Variation of heat transfer Co-efficient with time for both flat and wedge shaped micro-grooved copper plate has been shown in figure 4.12. It is obvious from figure 4.12 that the heat transfer Co-efficient for wedge shaped micro-grooved copper plate is increasing less compared to flat copper plate as the experiment time increases. In the case of wedge-shaped micro-grooved copper plate, this is owing to the formation of bigger droplets and an increase in surface rejuvenation time. As the rejuvenation time is increased, new vapor is prevented from coming into contact with the condensing surface, resulting in a slower condensation drainage rate and a reduced heat transfer coefficient. The larger droplets of modified plate offer more resistance to come into contact with condensing surfaces than thin liquid film formed at flat copper plate. The horizontal grooves of the leaf vein structure provide extra resistance along with the surface free energy to the falling droplets against the gravity, possibly resulting in a decreased heat transfer coefficient.

4.3.8 Effect of time on heat transfer Co-efficient for sinusoidal shaped micro-grooved copper plate

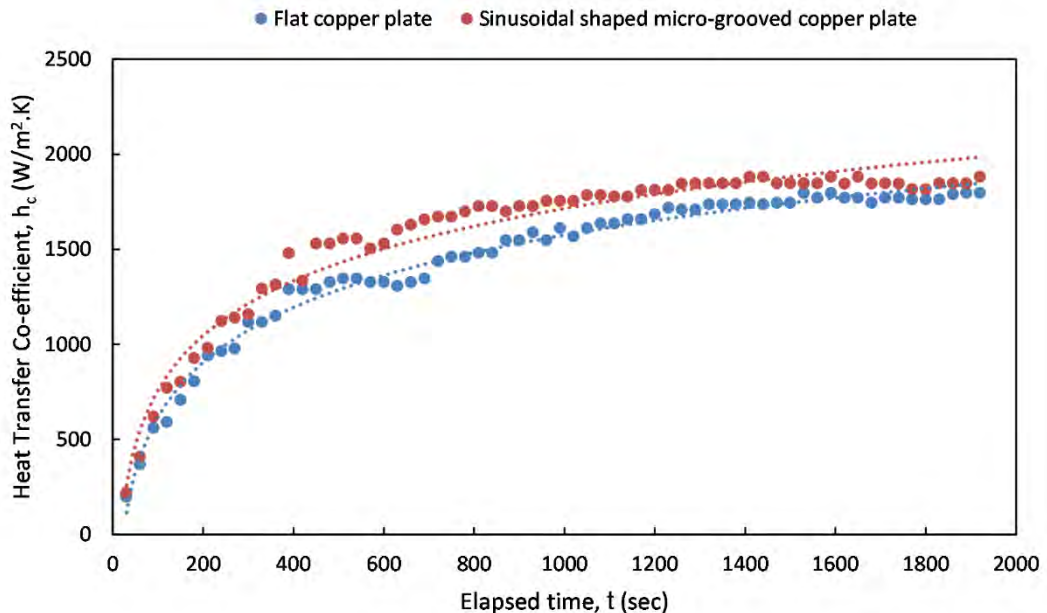


Figure 4.13: Variation of heat transfer Co-efficient with time for both flat and sinusoidal shaped micro-grooved copper plate

Figure 4.13 depicts the variation of heat transfer coefficient with time for both flat and sinusoidal shaped micro-grooved copper plates. Figure 4.13 shows that as the

experimental time goes on, the heat transfer Co-efficient of the sinusoidal shaped micro-grooved copper plate is noticeably higher than that of the flat copper plate. This is due to the appearance of larger droplets and the increment of rejuvenation time in case of flat copper plate. Increment of rejuvenation time refrains new vapor from coming into contact with condensing surface. The larger droplets of flat copper plate offer more resistance to come into contact with condensing surfaces. The falling droplets of sinusoidal shaped micro-grooved copper plate followed a parallel course between the grooves rather than being dispersed as they would on a flat plate. In the instance of a sinusoidal-shaped micro-grooved copper plate, this effect enhanced the sliding velocity of the falling droplets, resulting in a larger heat transfer coefficient.

4.3.9 Effect of time on heat transfer Co-efficient for rectangular shaped micro-grooved copper plate

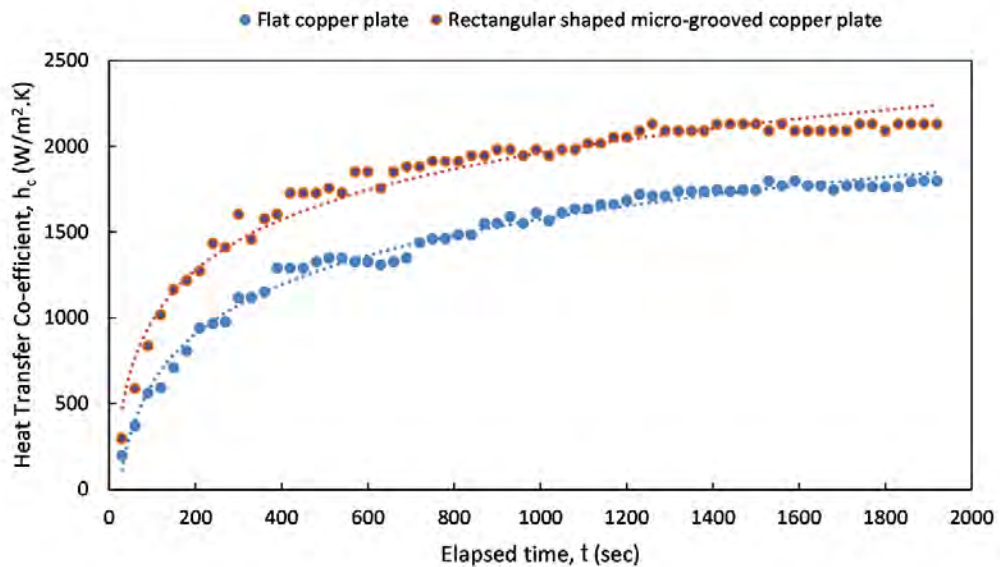


Figure 4.14: Variation of heat transfer Co-efficient with time for both flat and rectangular shaped micro-grooved copper plate

Figure 4.14 depicts the variation of heat transfer coefficient with time for both flat and rectangular shaped micro-grooved copper plates. Figure 4.14 shows that as the experiment time goes on, the heat transfer Co-efficient for rectangular shaped micro-grooved copper plate grows at a faster pace than flat copper plate. In the case of flat copper plates, this is due to the formation of larger droplets and an increase in surface rejuvenation time. The rejuvenation time is increased, which prevents new vapor from

coming into touch with the condensing surface. The larger droplets of flat copper plate offer more resistance to come into contact with condensing surfaces. Also, unlike flat plate, the falling droplets of rectangular shaped micro-grooved copper plate followed a parallel course between the grooves rather than being scattered. In the case of rectangular shaped micro-grooved copper plate, this phenomenon increased the sliding velocity of the falling droplets, resulting in a larger heat transfer coefficient.

4.3.10 Comparative analysis of effect of time on heat transfer Co-efficient of flat and modified copper surfaces

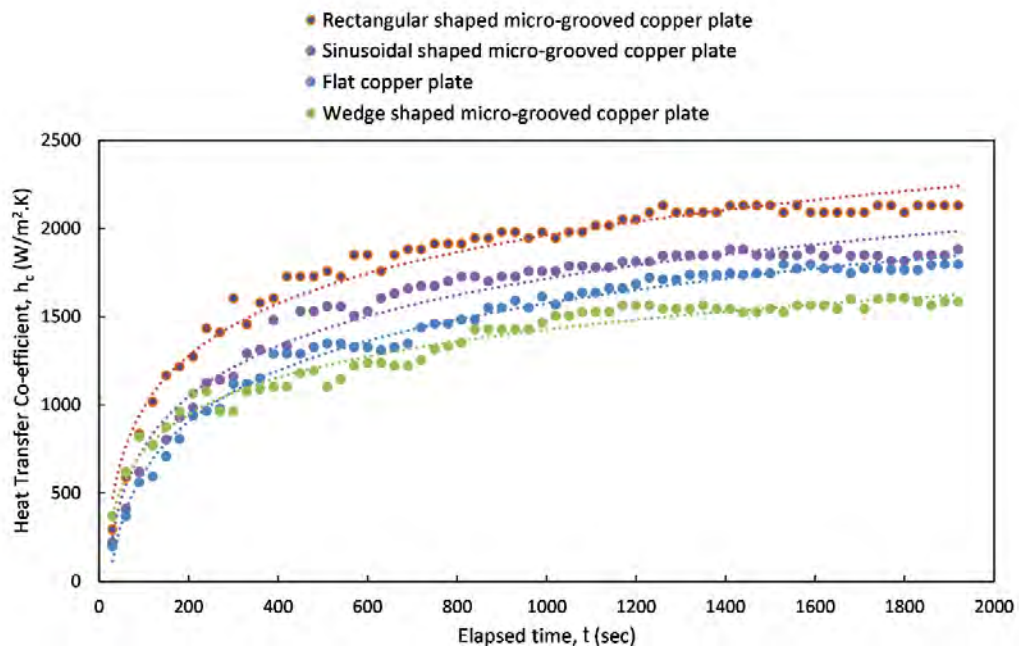


Figure 4.15: Variation of heat transfer Co-efficient with time for both flat and modified copper surfaces

The fluctuation of the heat transfer coefficient with time for both flat and modified copper surfaces is shown in Figure 4.15. From the comparative analysis it is obvious that the rectangular micro-grooved copper plate is less wettable than the other surfaces employed in this experiment. The higher contact angle, lower surface rejuvenation time, higher sliding velocity of droplets, etc. cause the rectangular micro-grooved copper plate to be more effective in terms of condensation heat transfer Co-efficient among other experimental surfaces. The wedge shaped micro-grooved copper plate, on the other hand, has a poorer heat transfer Co-efficient at a specific time due to the extended surface rejuvenation time and resistance caused by horizontal grooves.

CHAPTER 5: CONCLUSIONS

The findings of this thesis are summarized in this chapter. The study focuses on the effect of microgrooves on condensation heat transfer characteristics and compare it with that of the flat copper plate. Some possible future extension of research from this thesis is also proposed in this chapter.

5.1 Conclusion

In this study, wedge, sinusoidal and rectangular shaped micro-grooves have been precisely introduced on flat copper surface and then condensation heat transfer experiment has been performed for both flat and modified copper surfaces. The wettability, droplet morphology and the heat transfer characteristics of all surfaces have been investigated experimentally. Subsequently, the droplet formation, growth, coalescing and departure process from all the surfaces have been observed dynamically. The following contributions can be addressed from the above studies.

1. From the experimental results it is observed that the modified copper surfaces are less wettable compared to flat copper plate as contact angle of droplets on the modified surfaces are significantly larger than flat copper plate.
2. From the droplet morphology analysis, flat copper plate possesses almost 31% higher nucleation density compared to modified copper surfaces. The departed droplet diameter is 23% larger for the wedge shaped micro-grooved copper plate compared to flat plate. On the other hand, the departed droplet diameter for sinusoidal and rectangular shaped micro-grooved copper surfaces is 26% and 33% smaller than flat copper plate respectively.
3. The condensate drainage rate is 5% lower for wedge shaped micro-grooved copper plate than flat copper plate. This is due to the increment of falling droplet diameter and surface rejuvenation time in case of wedge shaped micro-grooved copper plate. For sinusoidal and rectangular shaped micro-grooved copper surfaces the condensate drainage rate is 9% and 12% higher

respectively compared to flat copper plate due to the decrement of departure diameter of falling droplets.

4. Heat transfer Co-efficient of wedge, sinusoidal and rectangular shaped micro-grooved surfaces are 15-18%, 15-50% and 20-60% higher than flat copper plate for the same Sub-cooling temperature. This is due to the decrement of wettability and droplet density in case of modified copper surfaces.
5. From the comparative analysis of droplet morphology and heat transfer behavior the rectangular micro-grooved copper surface possesses best condensation behavior among the grooved and flat surfaces studied.

5.2 Future Recommendations

There are some possible extensions to this thesis which should be pursued in order to shed more light on the condensation heat transfer behavior of copper surfaces. These are

- Wettability, droplet morphology and the heat transfer characteristics of nano materials coated grooved surfaces can be investigated further.
- The combined effect of porosity and micro-groove on condensation behavior of copper surfaces can be studied.
- Condensation heat transfer characteristics on wavy surfaces can also be studied further.

REFERENCES

1. Rose, J., Dropwise condensation theory and experiment: a review. Proceedings of the Institution of Mechanical Engineers, Part A: Journal of Power and Energy, 2002. 216(2): p. 115-128.
2. Das, A., et al., The use of an organic self-assembled monolayer coating to promote dropwise condensation of steam on horizontal tubes. J. Heat Transfer, 2000. 122(2): p. 278-286.
3. Tanner, D., et al., Heat transfer in dropwise condensation—Part I The effects of heat flux, steam velocity and non-condensable gas concentration. International Journal of Heat and Mass Transfer, 1965. 8(3): p. 419-426.
4. Stylianou, S. and J. Rose, Dropwise condensation on surfaces having different thermal conductivities. 1980.
5. Shigeo, H. and T. Hiroaki, Dropwise condensation of steam at low pressures. International journal of heat and mass transfer, 1987. 30(3): p. 497-507.
6. Kananeh, A.B., et al., Experimental study of dropwise condensation on plasma-ion implanted stainless steel tubes. International Journal of Heat and Mass Transfer, 2006. 49(25-26): p. 5018-5026.
7. Wen, R., et al., Droplet dynamics and heat transfer for dropwise condensation at lower and ultra-lower pressure. Applied Thermal Engineering, 2015. 88: p. 265-273.
8. Graham, C. and P. Griffith, Drop size distributions and heat transfer in dropwise condensation. International Journal of Heat and Mass Transfer, 1973. 16(2): p. 337-346.
9. Utaka, Y., et al., Transition from dropwise condensation to film condensation of propylene glycol, ethylene glycol, and glycerol vapors. Honolulu, HI: sn, 1987: p. 377-384.
10. Bonner III, R.W., Correlation for dropwise condensation heat transfer: Water, organic fluids, and inclination. International Journal of Heat and Mass Transfer, 2013. 61: p. 245-253.
11. Miljkovic, N., et al., Jumping-droplet-enhanced condensation on scalable superhydrophobic nanostructured surfaces. Nano letters, 2013. 13(1): p. 179-187.

12. Graham, C., The limiting heat transfer mechanisms of dropwise condensation. 1969, Massachusetts Institute of Technology.
13. Citakoglu, E. and J. Rose, Dropwise condensation—some factors influencing the validity of heat-transfer measurements. *International Journal of Heat and Mass Transfer*, 1968. 11(3): p. 523-537.
14. Le Fevre, E. and J.W. Rose. A theory of heat transfer by dropwise condensation. in *International Heat Transfer Conference Digital Library*. 1966. Begel House Inc.
15. McNeil, D.A., B. Burnside, and G. Cuthbertson, Dropwise condensation of steam on a small tube bundle at turbine condenser conditions. *Experimental Heat Transfer*, 2000. 13(2): p. 89-105.
16. Ma, X.-H., et al., Condensation heat transfer enhancement in the presence of non-condensable gas using the interfacial effect of dropwise condensation. *International Journal of Heat and Mass Transfer*, 2008. 51(7-8): p. 1728-1737.
17. Ma, X., et al. Dropwise condensation heat transfer on superhydrophobic surface in the presence of non-condensable gas. in *International Heat Transfer Conference*. 2010.
18. Ma, X., et al., Wetting mode evolution of steam dropwise condensation on superhydrophobic surface in the presence of noncondensable gas. *Journal of heat transfer*, 2012. 134(2).
19. McCormick, J. and J. Westwater, Nucleation sites for dropwise condensation. *Chemical Engineering Science*, 1965. 20(12): p. 1021-1036.
20. Tanasawa, I. and J.-i. Ochiai, Expeimental Study on Dropwise Condensatioin. *Bulletin of JSME*, 1973. 16(98): p. 1184-1197.
21. Leach, R., et al., Dropwise condensation: experiments and simulations of nucleation and growth of water drops in a cooling system. *Langmuir*, 2006. 22(21): p. 8864-8872.
22. Narhe, R. and D. Beysens, Growth dynamics of water drops on a square-pattern rough hydrophobic surface. *Langmuir*, 2007. 23(12): p. 6486-6489.
23. Young, T., III. An essay on the cohesion of fluids. *Philosophical transactions of the royal society of London*, 1805(95): p. 65-87.

24. Walpot, R., F. Ganzevles, and C. Van der Geld, Effects of contact angle on condensate topology, drainage and efficiency of a condenser with minichannels. *Experimental thermal and fluid science*, 2007. 31(8): p. 1033-1042.
25. Marto, P., et al., Evaluation of organic coatings for the promotion of dropwise condensation of steam. *International journal of heat and mass transfer*, 1986. 29(8): p. 1109-1117.
26. Aksan, S. and J. Rose, Dropwise condensation—the effect of thermal properties of the condenser material. *International Journal of Heat and Mass Transfer*, 1973. 16(2): p. 461-467.
27. Vemuri, S. and K. Kim, An experimental and theoretical study on the concept of dropwise condensation. *International journal of heat and mass transfer*, 2006. 49(3-4): p. 649-657.
28. Izumi, M., et al., Heat transfer enhancement of dropwise condensation on a vertical surface with round shaped grooves. *Experimental Thermal and Fluid Science*, 2004. 28(2-3): p. 243-248.
29. Peng, Q., et al., Influence of groove orientation on dropwise condensation on hydrophobic and hierarchical superhydrophobic surfaces with microgroove arrays. *International Communications in Heat and Mass Transfer*, 2020. 112: p. 104492.
30. Citakoglu, E. and J. Rose, Dropwise condensation—the effect of surface inclination. *International Journal of Heat and Mass Transfer*, 1969. 12(5): p. 645-651.
31. Liao, Q., et al., Experimental investigation of dropwise condensation heat transfer on the surface with a surface energy gradient. *Journal of Enhanced Heat Transfer*, 2007. 14(3).
32. Ghaffour, N., T.M. Missimer, and G.L. Amy, Technical review and evaluation of the economics of water desalination: current and future challenges for better water supply sustainability. *Desalination*, 2013. 309: p. 197-207.
33. Ghalavand, Y., M.S. Hatamipour, and A. Rahimi, A review on energy consumption of desalination processes. *Desalination and Water Treatment*, 2015. 54(6): p. 1526-1541.

34. Lukic, N., et al., Economical aspects of the improvement of a mechanical vapour compression desalination plant by dropwise condensation. *Desalination*, 2010. 264(1-2): p. 173-178.
35. Chung, S., K. Kadala, and H. Taylor, Stable dropwise condensation observed on a hierarchically structured superhydrophobic surface incorporating microdomes. *Microelectronic Engineering*, 2020. 225: p. 111252.
36. Garimella, S.V., Advances in mesoscale thermal management technologies for microelectronics. *Microelectronics Journal*, 2006. 37(11): p. 1165-1185.
37. Lee, A., et al., Water harvest via dewing. *Langmuir*, 2012. 28(27): p. 10183-10191.
38. Dehbi, A. and S. Guentay, A model for the performance of a vertical tube condenser in the presence of noncondensable gases. *Nuclear Engineering and Design*, 1997. 177(1-3): p. 41-52.
39. Kim, M.-H. and C.W. Bullard, Air-side performance of brazed aluminum heat exchangers under dehumidifying conditions. *International Journal of refrigeration*, 2002. 25(7): p. 924-934.
40. Seo, D., C. Lee, and Y. Nam, Influence of geometric patterns of microstructured superhydrophobic surfaces on water-harvesting performance via dewing. *Langmuir*, 2014. 30(51): p. 15468-15476.
41. Hong, K. and R. Webb, Performance of dehumidifying heat exchangers with and without wetting coatings. 1999.
42. Attinger, D., et al., Surface engineering for phase change heat transfer: A review. *MRS Energy & Sustainability*, 2014. 1.
43. Schmidt, E., W. Schurig, and W. Sellschopp, Versuche über die Kondensation von Wasserdampf in Film-und Tropfenform. *Technische Mechanik und Thermodynamik*, 1930. 1(2): p. 53-63.
44. Zhao, Q., et al., Dropwise condensation on LB film surface. *Chemical Engineering and Processing: Process Intensification*, 1996. 35(6): p. 473-477.
45. Li, Q., et al., Lattice Boltzmann modeling of boiling heat transfer: The boiling curve and the effects of wettability. *International Journal of Heat and Mass Transfer*, 2015. 85: p. 787-796.

46. Carey, V.P., *Liquid-vapor phase-change phenomena: an introduction to the thermophysics of vaporization and condensation processes in heat transfer equipment*. 2020: CRC Press.
47. Rose, J. and L. Glicksman, Dropwise condensation—the distribution of drop sizes. *International Journal of Heat and Mass Transfer*, 1973. 16(2): p. 411-425.
48. Yamada, Y., et al., Droplet nucleation on a well-defined hydrophilic–hydrophobic surface of 10 nm order resolution. *Langmuir*, 2014. 30(48): p. 14532-14537.
49. Patankar, N.A., Supernucleating surfaces for nucleate boiling and dropwise condensation heat transfer. *Soft Matter*, 2010. 6(8): p. 1613-1620.
50. Anand, S., et al., Enhanced condensation on lubricant-impregnated nanotextured surfaces. *ACS nano*, 2012. 6(11): p. 10122-10129.
51. Vorobyev, A. and C. Guo, Multifunctional surfaces produced by femtosecond laser pulses. *Journal of Applied Physics*, 2015. 117(3): p. 033103.
52. Chau, T., et al., A review of factors that affect contact angle and implications for flotation practice. *Advances in colloid and interface science*, 2009. 150(2): p. 106-115.
53. Orlova, E., D. Feoktistov, and G. Kuznetsov. Investigation of drop dynamic contact angle on copper surface. in *EPJ Web of Conferences*. 2015. EDP Sciences.
54. Zhong, L., et al., Effects of surface free energy and nanostructures on dropwise condensation. *Chemical engineering journal*, 2010. 156(3): p. 546-552.
55. Chatterjee, A., et al., Condensation heat transfer on patterned surfaces. *International Journal of Heat and Mass Transfer*, 2013. 66: p. 889-897.
56. Chatterjee, A., et al., Enhancement of condensation heat transfer with patterned surfaces. *International Journal of Heat and Mass Transfer*, 2014. 71: p. 675-681.
57. Peng, B., et al., Experimental investigation on steam condensation heat transfer enhancement with vertically patterned hydrophobic–hydrophilic hybrid surfaces. *International Journal of Heat and Mass Transfer*, 2015. 83: p. 27-38.

58. Varanasi, K.K., et al., Spatial control in the heterogeneous nucleation of water. *Applied Physics Letters*, 2009. 95(9): p. 094101.
59. Hou, Y., et al., Recurrent filmwise and dropwise condensation on a beetle mimetic surface. *ACS nano*, 2015. 9(1): p. 71-81.
60. Daniel, S., M.K. Chaudhury, and J.C. Chen, Fast drop movements resulting from the phase change on a gradient surface. *Science*, 2001. 291(5504): p. 633-636.
61. Ghosh, A., et al., Enhancing dropwise condensation through bioinspired wettability patterning. *Langmuir*, 2014. 30(43): p. 13103-13115.
62. Tanasawa, I., J. Ochiai, and Y. Funawatashi. Experimental study on dropwise condensation– effect of maximum drop size upon the heat transfer coefficient. in *International Heat Transfer Conference Digital Library*. 1978. Begel House Inc.
63. Watanabe, K., Y. Udagawa, and H. Udagawa, Drag reduction of Newtonian fluid in a circular pipe with a highly water-repellent wall. *Journal of Fluid Mechanics*, 1999. 381: p. 225-238.
64. Sommers, A. and A. Jacobi, Wetting phenomena on micro-grooved aluminum surfaces and modeling of the critical droplet size. *Journal of colloid and interface science*, 2008. 328(2): p. 402-411.
65. Dietz, C., et al., Visualization of droplet departure on a superhydrophobic surface and implications to heat transfer enhancement during dropwise condensation. *Applied physics letters*, 2010. 97(3): p. 033104.
66. Boreyko, J.B. and C.-H. Chen, Self-propelled dropwise condensate on superhydrophobic surfaces. *Physical review letters*, 2009. 103(18): p. 184501.
67. Miljkovic, N. and E.N. Wang, Condensation heat transfer on superhydrophobic surfaces. *MRS bulletin*, 2013. 38(5): p. 397-406.
68. Li, P., et al., Anisotropic wetting properties on a precision-ground micro-V-grooved Si surface related to their micro-characterized variables. *Journal of Micromechanics and Microengineering*, 2014. 24(7): p. 075004.
69. Zamuruyev, K.O., et al., Continuous droplet removal upon dropwise condensation of humid air on a hydrophobic micropatterned surface. *Langmuir*, 2014. 30(33): p. 10133-10142.

70. Lu, C.-H., et al., Heat transfer model of dropwise condensation and experimental validation for surface with coating and groove at low pressure. *Heat and Mass Transfer*, 2016. 52(1): p. 113-126.
71. Lara, J.R. and M.T. Holtzapfle, Experimental investigation of dropwise condensation on hydrophobic heat exchangers. Part II: Effect of coatings and surface geometry. *Desalination*, 2011. 280(1-3): p. 363-369.
72. Qi, B., et al., Study on the wettability and condensation heat transfer of sine-shaped micro-grooved surfaces. *Experimental Thermal and Fluid Science*, 2018. 90: p. 28-36.
73. Malik, F., et al., Nature's moisture harvesters: a comparative review. *Bioinspiration & biomimetics*, 2014. 9(3): p. 031002.
74. Nørgaard, T., M. Ebner, and M. Dacke, Animal or plant: which is the better fog water collector? *PloS one*, 2012. 7(4): p. e34603.
75. Thickett, S.C., C. Neto, and A.T. Harris, Biomimetic surface coatings for atmospheric water capture prepared by dewetting of polymer films. *Advanced Materials*, 2011. 23(32): p. 3718-3722.
76. Nusselt, W., Die oberflächenkondensation des wasserdampfes zeitschrift. 1916, VDI.
77. Niu, D., et al., Dropwise condensation heat transfer model considering the liquid-solid interfacial thermal resistance. *International Journal of Heat and Mass Transfer*, 2017. 112: p. 333-342.
78. Liu, X. and P. Cheng, Dropwise condensation theory revisited Part II. Droplet nucleation density and condensation heat flux. *International Journal of Heat and Mass Transfer*, 2015. 83: p. 842-849.
79. Rose, J., Fundamentals of condensation heat transfer: Laminar film condensation. *JSME international journal. Ser. 2, Fluids engineering, heat transfer, power, combustion, thermophysical properties*, 1988. 31(3): p. 357-375.
80. Memory, S., V. Adams, and P. Marto, Free and forced convection laminar film condensation on horizontal elliptical tubes. *International journal of heat and mass transfer*, 1997. 40(14): p. 3395-3406.

81. Khandekar, S. and K. Muralidhar, Dropwise condensation on inclined textured surfaces. 2014: Springer.
82. Leipertz, A., J3 Dropwise Condensation: Datasheet from VDI-Buch · Volume : "VDI Heat Atlas" in SpringerMaterials (https://doi.org/10.1007/978-3-540-77877-6_61). Springer-Verlag.
83. Umur, A. and P. Griffith, Mechanism of Dropwise Condensation. Journal of Heat Transfer, 1965. 87(2): p. 275-282.
84. Station, U.o.I.E.E. and M. Jakob, Heat transfer in evaporation and condensation. 1937.
85. Yongji, S., et al., A study on the mechanism of dropwise condensation. International journal of heat and mass transfer, 1991. 34(11): p. 2827-2831.
86. Welch, J.F., Microscopic study of dropwise condensation. 1961: University of Illinois at Urbana-Champaign.
87. Sugawara, S. and K. Katsuta. Fundamental study on dropwise condensation. in International Heat Transfer Conference Digital Library. 1966. Begel House Inc.
88. Eucken, A.v., Energie-und stoffaustausch an grenzflächen. Naturwissenschaften, 1937. 25(14): p. 209-218.
89. Rose, J., Y. Utaka, and I. Tanasawa, Dropwise condensation: in Handbook of Phase Change: Boling and Condensation. 1999, USA: Taylor and Francis.
90. Tanaka, H., A theoretical study of dropwise condensation. 1975.
91. Rose, J.W. Interphase matter transfer, the condensation coefficient and dropwise condensation. in International Heat Transfer Conference Digital Library. 1998. Begel House Inc.
92. Gose, E.E., A. Mucciardi, and E. Baer, Model for dropwise condensation on randomly distributed sites. International Journal of Heat and Mass Transfer, 1967. 10(1): p. 15-22.
93. Silver, R., An approach to a general theory of surface condensers. Proceedings of the Institution of Mechanical Engineers, 1963. 178(1): p. 339-357.
94. Morris, A.S., Measurement and instrumentation principles. 2001, IOP Publishing.

95. Leu, T.-S., H.-W. Lin, and T.-H. Wu, Applications of surface modification techniques in enhancement of phase change heat transfer. *Modern Physics Letters B*, 2010. 24(13): p. 1381-1384.
96. Huang, D.-J. and T.-S. Leu, Condensation heat transfer enhancement by surface modification on a monolithic copper *heat sink*. *Applied Thermal Engineering*, 2015. 75: p. 908-917.

APPENDIX

Appendix-1: Experimental data for flat copper plate

Table 3: Experimental data for flat copper plate

Time t (sec)	Upper surface temperature T ₁ (°C)	Lower surface temperature T ₃ (°C)	Cooling water inlet temperature T ₅ (°C)	Cooling water outlet temperature T ₂ (°C)	Steam inlet temperature T ₄ (°C)
30	37	49	25	28	100
60	45	53	25	30	100
90	50	56	25	32	100
120	53	58	25	32	100
150	55	60	25	33	100
180	56	60	25	34	100
210	59	61	25	35	100
240	61	61	25	35	100
270	61	62	25	35	100
300	64	62	25	36	100
330	64	62	25	36	100
360	66	62	25	36	100
390	67	63	25	37	100
420	67	63	25	37	100
450	67	63	25	37	100
480	69	63	25	37	100
510	69	64	25	37	100
540	69	64	25	37	100
570	69	63	25	37	100
600	69	63	25	37	100
630	69	62	25	37	100

660	68	64	25	37	100
690	69	64	25	37	100
720	69	63	25	38	100
750	70	63	25	38	100
780	69	64	25	38	100
810	69	65	25	38	100
840	69	65	25	38	100
870	68	64	25	39	100
900	68	64	25	39	100
930	67	62	25	40	100
960	68	64	25	39	100
990	67	63	25	40	100
1020	66	62	25	40	100
1050	67	63	25	40	100
1080	67	64	25	40	100
1110	66	65	25	40	100
1140	67	65	25	40	100
1170	67	65	25	40	100
1200	68	65	25	40	100
1230	67	63	25	41	100
1260	69	65	25	40	100
1290	69	65	25	40	100
1320	70	65	25	40	100
1350	70	65	25	40	100
1380	70	65	25	40	100
1410	68	63	25	41	100
1440	70	65	25	40	100
1470	68	63	25	41	100
1500	68	63	25	41	100
1530	69	64	25	41	100
1560	68	64	25	41	100

1590	69	64	25	41	100
1620	69	63	25	41	100
1650	69	63	25	41	100
1680	68	63	25	41	100
1710	68	64	25	41	100
1740	67	65	25	41	100
1770	70	66	25	40	100
1800	70	66	25	40	100
1830	70	66	25	40	100
1860	71	66	25	40	100
1890	68	65	25	41	100
1920	68	65	25	41	100

Table 4: Calculation of area and mass flow rate for flat copper plate

Total time of water collection	Effective condensation heat transfer area	Mass of water collected	Mass flow rate of water
t (sec)	A (m ²)	m (kg)	ṁ (kg/sec)
180	0.016	2.588	0.01438

Table 5: Calculation of heat flux for flat copper plate

Upper surface temperature T ₁ (°C)	Lower surface temperature T ₃ (°C)	Cooling water inlet temperature T ₅ (°C)	Cooling water outlet temperature T ₂ (°C)	Calculated heat flux q (W/m ²)
37	49	25	28	11283.81
45	53	25	30	18806.34
50	56	25	32	26328.88

53	58	25	32	26328.88
55	60	25	33	30090.15
56	60	25	34	33851.42
59	61	25	35	37612.69
61	61	25	35	37612.69
61	62	25	35	37612.69
64	62	25	36	41373.96
64	62	25	36	41373.96
66	62	25	36	41373.96
67	63	25	37	45135.23
67	63	25	37	45135.23
67	63	25	37	45135.23
69	63	25	37	45135.23
69	64	25	37	45135.23
69	64	25	37	45135.23
69	63	25	37	45135.23
69	63	25	37	45135.23
69	62	25	37	45135.23
68	64	25	37	45135.23
69	64	25	37	45135.23
69	63	25	38	48896.49
70	63	25	38	48896.49
69	64	25	38	48896.49
69	65	25	38	48896.49
69	65	25	38	48896.49
68	64	25	39	52657.76
68	64	25	39	52657.76
67	62	25	40	56419.03
68	64	25	39	52657.76
67	63	25	40	56419.03
66	62	25	40	56419.03

67	63	25	40	56419.03
67	64	25	40	56419.03
66	65	25	40	56419.03
67	65	25	40	56419.03
67	65	25	40	56419.03
68	65	25	40	56419.03
67	63	25	41	60180.3
69	65	25	40	56419.03
69	65	25	40	56419.03
70	65	25	40	56419.03
70	65	25	40	56419.03
70	65	25	40	56419.03
68	63	25	41	60180.3
70	65	25	40	56419.03
68	63	25	41	60180.3
68	63	25	41	60180.3
69	64	25	41	60180.3
68	64	25	41	60180.3
69	64	25	41	60180.3
69	63	25	41	60180.3
69	63	25	41	60180.3
68	63	25	41	60180.3
68	64	25	41	60180.3
67	65	25	41	60180.3
70	66	25	40	56419.03
70	66	25	40	56419.03
70	66	25	40	56419.03
71	66	25	40	56419.03
68	65	25	41	60180.3
68	65	25	41	60180.3

Table 6: Calculation of heat transfer Co-efficient for flat copper plate

Calculated heat flux q (W/m ²)	Steam inlet temperature T ₄ (°C)	Surface temperature of copper plate T _{surf} (°C)	Temperature difference ΔT (°C)	Heat transfer Co-efficient h _c (W/m ² .°C)
11283.81	100	43	57	197.96
18806.34	100	49	51	368.75
26328.88	100	53	47	560.18
26328.88	100	55.5	44.5	591.66
30090.15	100	57.5	42.5	708.00
33851.42	100	58	42	805.98
37612.69	100	60	40	940.31
37612.69	100	61	39	964.42
37612.69	100	61.5	38.5	976.95
41373.96	100	63	37	1118.21
41373.96	100	63	37	1118.21
41373.96	100	64	36	1149.27
45135.23	100	65	35	1289.57
45135.23	100	65	35	1289.57
45135.23	100	65	35	1289.57
45135.23	100	66	34	1327.50
45135.23	100	66.5	33.5	1347.32
45135.23	100	66.5	33.5	1347.32
45135.23	100	66	34	1327.50
45135.23	100	66	34	1327.50
45135.23	100	65.5	34.5	1308.26
45135.23	100	66	34	1327.50

45135.23	100	66.5	33.5	1347.32
48896.49	100	66	34	1438.13
48896.49	100	66.5	33.5	1459.59
48896.49	100	66.5	33.5	1459.59
48896.49	100	67	33	1481.71
48896.49	100	67	33	1481.71
52657.76	100	66	34	1548.75
52657.76	100	66	34	1548.75
56419.03	100	64.5	35.5	1589.26
52657.76	100	66	34	1548.75
56419.03	100	65	35	1611.97
56419.03	100	64	36	1567.19
56419.03	100	65	35	1611.97
56419.03	100	65.5	34.5	1635.33
56419.03	100	65.5	34.5	1635.33
56419.03	100	66	34	1659.38
56419.03	100	66	34	1659.38
56419.03	100	66.5	33.5	1684.15
60180.3	100	65	35	1719.43
56419.03	100	67	33	1709.66
56419.03	100	67	33	1709.66
56419.03	100	67.5	32.5	1735.97
56419.03	100	67.5	32.5	1735.97
56419.03	100	67.5	32.5	1735.97
60180.30	100	65.5	34.5	1744.35
56419.03	100	67.5	32.5	1735.97
60180.30	100	65.5	34.5	1744.35
60180.30	100	65.5	34.5	1744.35
60180.30	100	66.5	33.5	1796.42

60180.30	100	66	34	1770.00
60180.30	100	66.5	33.5	1796.42
60180.30	100	66	34	1770.00
60180.30	100	66	34	1770.00
60180.30	100	65.5	34.5	1744.35
60180.30	100	66	34	1770.00
60180.30	100	66	34	1770.00
56419.03	100	68	32	1763.09
56419.03	100	68	32	1763.09
56419.03	100	68	32	1763.09
56419.03	100	68.5	31.5	1791.08
60180.30	100	66.5	33.5	1796.42
60180.30	100	66.5	33.5	1796.42

Appendix-2: Experimental data for wedge shaped micro-grooved copper plate

Table 7: Experimental data for wedge shaped micro-grooved copper plate

Time t (sec)	Upper surface temperature T ₁ (°C)	Lower surface temperature T ₃ (°C)	Cooling water inlet temperature T ₅ (°C)	Cooling water outlet temperature T ₂ (°C)	Steam inlet temperature T ₄ (°C)
30	43	55	26	31	100
60	47	56	26	34	100
90	50	58	26	36	100
120	52	60	26	35	100
150	54	60	26	36	100
180	54	60	26	37	100
210	54	61	26	38	100
240	55	61	26	38	100
270	54	60	26	37	100
300	54	60	26	37	100
330	55	61	26	38	100
360	56	61	26	38	100
390	56	62	26	38	100
420	56	62	26	38	100
450	55	62	26	39	100
480	56	62	26	39	100
510	56	62	26	38	100
540	57	64	26	38	100
570	56	64	26	39	100
600	57	64	26	39	100
630	57	64	26	39	100
660	58	62	26	39	100
690	58	62	26	39	100

720	56	60	26	40	100
750	57	63	26	40	100
780	57	64	26	40	100
810	58	64	26	40	100
840	57	64	26	41	100
870	57	64	26	41	100
900	57	64	26	41	100
930	57	64	26	41	100
960	57	64	26	41	100
990	58	65	26	41	100
1020	56	64	26	42	100
1050	56	64	26	42	100
1080	56	65	26	42	100
1110	60	66	26	41	100
1140	60	66	26	41	100
1170	59	64	26	42	100
1200	59	64	26	42	100
1230	59	64	26	42	100
1260	58	64	26	42	100
1290	58	64	26	42	100
1320	58	64	26	42	100
1350	58	65	26	42	100
1380	58	64	26	42	100
1410	58	64	26	42	100
1440	57	64	26	42	100
1470	57	64	26	42	100
1500	58	64	26	42	100
1530	57	64	26	42	100
1560	58	65	26	42	100
1590	58	65	26	42	100
1620	58	65	26	42	100

1650	58	64	26	42	100
1680	57	63	26	43	100
1710	58	64	26	42	100
1740	57	63	26	43	100
1770	59	66	26	42	100
1800	59	66	26	42	100
1830	59	65	26	42	100
1860	58	65	26	42	100
1890	59	65	26	42	100
1920	58	66	26	42	100

Table 8: Calculation of area and mass flow rate for wedge shaped micro-grooved copper plate

Total time of water collection	Effective condensation heat transfer area	Mass of water collected	Mass flow rate of water
t (sec)	A (m ²)	m (kg)	\dot{m} (kg/sec)
180	0.016	2.588	0.01438

Table 9: Calculation of heat flux for wedge shaped micro-grooved copper plate

Upper surface temperature T ₁ (°C)	Lower surface temperature T ₃ (°C)	Cooling water inlet temperature T ₅ (°C)	Cooling water outlet temperature T ₂ (°C)	Calculated heat flux q (W/m ²)
43	55	26	31	18806.34
47	56	26	34	30090.15
50	58	26	36	37612.68
52	60	26	35	33851.41
54	60	26	36	37612.68

54	60	26	37	41373.95
54	61	26	38	45135.22
55	61	26	38	45135.22
54	60	26	37	41373.95
54	60	26	37	41373.95
55	61	26	38	45135.22
56	61	26	38	45135.22
56	62	26	38	45135.22
56	62	26	38	45135.22
55	62	26	39	48896.49
56	62	26	39	48896.49
56	62	26	38	45135.22
57	64	26	38	45135.22
56	64	26	39	48896.49
57	64	26	39	48896.49
57	64	26	39	48896.49
58	62	26	39	48896.49
58	62	26	39	48896.49
56	60	26	40	52657.76
57	63	26	40	52657.76
57	64	26	40	52657.76
58	64	26	40	52657.76
57	64	26	41	56419.03
57	64	26	41	56419.03
57	64	26	41	56419.03
57	64	26	41	56419.03
57	64	26	41	56419.03
58	65	26	41	56419.03
56	64	26	42	60180.3
56	64	26	42	60180.3
56	65	26	42	60180.3

60	66	26	41	56419.0
60	66	26	41	56419.0
59	64	26	42	60180.3
59	64	26	42	60180.3
59	64	26	42	60180.3
58	64	26	42	60180.3
58	64	26	42	60180.3
58	64	26	42	60180.3
58	65	26	42	60180.3
58	64	26	42	60180.3
58	64	26	42	60180.3
57	64	26	42	60180.3
57	64	26	42	60180.3
58	64	26	42	60180.3
57	64	26	42	60180.3
58	65	26	42	60180.3
58	65	26	42	60180.3
58	65	26	42	60180.3
58	64	26	42	60180.3
57	63	26	43	63941.5
58	64	26	42	60180.3
57	63	26	43	63941.5
59	66	26	42	60180.3
59	66	26	42	60180.3
59	65	26	42	60180.3
58	65	26	42	60180.3
59	65	26	42	60180.3
58	66	26	42	60180.3

Table 10: Calculation of heat transfer Co-efficient for wedge shaped micro-grooved copper plate

Calculated heat flux q (W/m ²)	Steam inlet temperature T_4 (°C)	Surface temperature of copper plate T_{surf} (°C)	Temperature difference ΔT (°C)	Heat transfer Co-efficient h_c (W/m ² .°C)
18806.34	100	49	51	368.75
30090.15	100	51.5	48.5	620.41
37612.68	100	54	46	817.66
33851.41	100	56	44	769.35
37612.68	100	57	43	874.71
41373.95	100	57	43	962.18
45135.22	100	57.5	42.5	1062.00
45135.22	100	58	42	1074.64
41373.95	100	57	43	962.18
41373.95	100	57	43	962.18
45135.22	100	58	42	1074.64
45135.22	100	58.5	41.5	1087.59
45135.22	100	59	41	1100.85
45135.22	100	59	41	1100.85
48896.49	100	58.5	41.5	1178.22
48896.49	100	59	41	1192.59
45135.22	100	59	41	1100.85
45135.22	100	60.5	39.5	1142.66
48896.49	100	60	40	1222.41
48896.49	100	60.5	39.5	1237.88
48896.49	100	60.5	39.5	1237.88
48896.49	100	60	40	1222.41

48896.49	100	60	40	1222.41
52657.76	100	58	42	1253.75
52657.76	100	60	40	1316.44
52657.76	100	60.5	39.5	1333.10
52657.76	100	61	39	1350.19
56419.03	100	60.5	39.5	1428.32
56419.03	100	60.5	39.5	1428.32
56419.03	100	60.5	39.5	1428.32
56419.03	100	60.5	39.5	1428.32
56419.03	100	60.5	39.5	1428.32
56419.03	100	60.5	39.5	1428.32
56419.03	100	61.5	38.5	1465.42
60180.30	100	60	40	1504.50
60180.30	100	60	40	1504.50
60180.30	100	60.5	39.5	1523.55
56419.031	100	63	37	1524.83
56419.031	100	63	37	1524.83
60180.30	100	61.5	38.5	1563.12
60180.30	100	61.5	38.5	1563.12
60180.30	100	61.5	38.5	1563.12
60180.30	100	61	39	1543.08
60180.30	100	61	39	1543.08
60180.30	100	61	39	1543.08
60180.30	100	61.5	38.5	1563.12
60180.30	100	61	39	1543.08
60180.30	100	61	39	1543.08
60180.30	100	60.5	39.5	1523.55
60180.30	100	60.5	39.5	1523.55
60180.30	100	61	39	1543.08
60180.30	100	60.5	39.5	1523.55
60180.30	100	61.5	38.5	1563.12
60180.30	100	61.5	38.5	1563.12

60180.30	100	61.5	38.5	1563.12
60180.30	100	61	39	1543.08
63941.56	100	60	40	1598.53
60180.30	100	61	39	1543.08
63941.56	100	60	40	1598.53
60180.30	100	62.5	37.5	1604.80
60180.30	100	62.5	37.5	1604.80
60180.30	100	62	38	1583.69
60180.30	100	61.5	38.5	1563.12
60180.30	100	62	38	1583.69
60180.30	100	62	38	1583.69

Appendix-3: Experimental data for sinusoidal shaped micro-grooved copper plate

Table 11: Experimental data for sinusoidal shaped micro-grooved copper plate

Time t (sec)	Upper surface temperature T ₁ (°C)	Lower surface temperature T ₃ (°C)	Cooling water inlet temperature T ₅ (°C)	Cooling water outlet temperature T ₂ (°C)	Steam inlet temperature T ₄ (°C)
30	37	60	28	31	100
60	45	63	28	33	100
90	50	65	28	35	100
120	55	67	28	36	100
150	58	67	28	36	100
180	60	67	28	37	100
210	63	68	28	37	100
240	65	68	28	38	100
270	66	68	28	38	100
300	67	68	28	38	100
330	68	68	28	39	100
360	68	69	28	39	100
390	69	70	28	40	100
420	70	68	28	39	100
450	71	70	28	40	100
480	71	70	28	40	100
510	72	70	28	40	100
540	72	70	28	40	100
570	72	68	28	40	100
600	71	70	28	40	100
630	70	69	28	41	100
660	70	70	28	41	100

690	72	69	28	41	100
720	70	67	28	42	100
750	70	67	28	42	100
780	71	67	28	42	100
810	72	67	28	42	100
840	72	67	28	42	100
870	71	67	28	42	100
900	72	67	28	42	100
930	71	68	28	42	100
960	71	69	28	42	100
990	71	69	28	42	100
1020	72	68	28	42	100
1050	72	69	28	42	100
1080	72	69	28	42	100
1110	74	71	28	41	100
1140	74	71	28	41	100
1170	74	72	28	41	100
1200	74	72	28	41	100
1230	75	71	28	41	100
1260	75	72	28	41	100
1290	73	70	28	42	100
1320	73	70	28	42	100
1350	73	70	28	42	100
1380	72	71	28	42	100
1410	73	71	28	42	100
1440	73	71	28	42	100
1470	73	70	28	42	100
1500	72	71	28	42	100
1530	73	70	28	42	100
1560	73	70	28	42	100
1590	73	71	28	42	100

1620	75	72	28	41	100
1650	74	70	28	42	100
1680	75	72	28	41	100
1710	73	70	28	42	100
1740	75	72	28	41	100
1770	73	69	28	42	100
1800	72	70	28	42	100
1830	74	69	28	42	100
1860	75	68	28	42	100
1890	74	69	28	42	100
1920	75	69	28	42	100

Table 12: Calculation of area and mass flow rate for sinusoidal shaped micro-grooved copper plate

Total time of water collection	Effective condensation heat transfer area	Mass of water collected	Mass flow rate of water
t (sec)	A (m ²)	m (kg)	\dot{m} (kg/sec)
180	0.016	2.588	0.01438

Table 13: Calculation of heat flux for sinusoidal shaped micro-grooved copper plate

Upper surface temperature T_1 (°C)	Lower surface temperature T_3 (°C)	Cooling water inlet temperature T_5 (°C)	Cooling water outlet temperature T_2 (°C)	Calculated heat flux q (W/m ²)
37	60	28	31	11283.81
45	63	28	33	18806.34
50	65	28	35	26328.88
55	67	28	36	30090.15

58	67	28	36	30090.15
60	67	28	37	33851.42
63	68	28	37	33851.42
65	68	28	38	37612.69
66	68	28	38	37612.69
67	68	28	38	37612.69
68	68	28	39	41373.96
68	69	28	39	41373.96
69	70	28	40	45135.23
70	68	28	39	41373.96
71	70	28	40	45135.23
71	70	28	40	45135.23
72	70	28	40	45135.23
72	70	28	40	45135.23
72	68	28	40	45135.23
71	70	28	40	45135.23
70	69	28	41	48896.49
70	70	28	41	48896.49
72	69	28	41	48896.49
70	67	28	42	52657.76
70	67	28	42	52657.76
71	67	28	42	52657.76
72	67	28	42	52657.76
72	67	28	42	52657.76
71	67	28	42	52657.76
72	67	28	42	52657.76
71	68	28	42	52657.76
71	69	28	42	52657.76
71	69	28	42	52657.76
72	68	28	42	52657.76
72	69	28	42	52657.76

72	69	28	42	52657.76
74	71	28	41	48896.49
74	71	28	41	48896.49
74	72	28	41	48896.49
74	72	28	41	48896.49
75	71	28	41	48896.49
75	72	28	41	48896.49
73	70	28	42	52657.76
73	70	28	42	52657.76
73	70	28	42	52657.76
72	71	28	42	52657.76
73	71	28	42	52657.76
73	71	28	42	52657.76
73	70	28	42	52657.76
72	71	28	42	52657.76
73	70	28	42	52657.76
73	70	28	42	52657.76
73	71	28	42	52657.76
75	72	28	41	48896.49
74	70	28	42	52657.76
75	72	28	41	48896.49
73	70	28	42	52657.76
75	72	28	41	48896.49
73	69	28	42	52657.76
72	70	28	42	52657.76
74	69	28	42	52657.76
75	68	28	42	52657.76
74	69	28	42	52657.76
75	69	28	42	52657.76

Table 14: Calculation of heat transfer Co-efficient for sinusoidal shaped micro-grooved copper plate

Calculated heat flux q (W/m^2)	Steam inlet temperature T_4 ($^{\circ}C$)	Surface temperature of copper plate T_{surf} ($^{\circ}C$)	Temperature difference ΔT ($^{\circ}C$)	Heat transfer Co-efficient h_c ($W/m^2 \cdot ^{\circ}C$)
11283.81	100	48.5	51.5	219.10
18806.34	100	54	46	408.83
26328.88	100	57.5	42.5	619.50
30090.15	100	61	39	771.54
30090.15	100	62.5	37.5	802.40
33851.42	100	63.5	36.5	927.43
33851.42	100	65.5	34.5	981.20
37612.69	100	66.5	33.5	1122.76
37612.69	100	67	33	1139.77
37612.69	100	67.5	32.5	1157.31
41373.96	100	68	32	1292.93
41373.96	100	68.5	31.5	1313.45
45135.23	100	69.5	30.5	1479.84
41373.96	100	69	31	1334.64
45135.23	100	70.5	29.5	1530.00
45135.23	100	70.5	29.5	1530.00
45135.23	100	71	29	1556.38
45135.23	100	71	29	1556.38
45135.23	100	70	30	1504.50
45135.23	100	70.5	29.5	1530.00
48896.49	100	69.5	30.5	1603.16
48896.49	100	70	30	1629.88

48896.49	100	70.5	29.5	1657.50
52657.76	100	68.5	31.5	1671.67
52657.76	100	68.5	31.5	1671.67
52657.76	100	69	31	1698.63
52657.76	100	69.5	30.5	1726.48
52657.76	100	69.5	30.5	1726.48
52657.76	100	69	31	1698.63
52657.76	100	69.5	30.5	1726.48
52657.76	100	69.5	30.5	1726.48
52657.76	100	70	30	1755.25
52657.76	100	70	30	1755.25
52657.76	100	70	30	1755.25
52657.76	100	70.5	29.5	1785.00
52657.76	100	70.5	29.5	1785.00
48896.49	100	72.5	27.5	1778.05
48896.49	100	72.5	27.5	1778.05
48896.49	100	73	27	1810.98
48896.49	100	73	27	1810.98
48896.49	100	73	27	1810.98
48896.49	100	73.5	26.5	1845.15
52657.76	100	71.5	28.5	1847.64
52657.76	100	71.5	28.5	1847.64
52657.76	100	71.5	28.5	1847.64
52657.76	100	71.5	28.5	1847.64
52657.76	100	72	28	1880.63
52657.76	100	72	28	1880.63
52657.76	100	71.5	28.5	1847.64
52657.76	100	71.5	28.5	1847.64
52657.76	100	71.5	28.5	1847.64
52657.76	100	71.5	28.5	1847.64
52657.76	100	72	28	1880.63

48896.49	100	73.5	26.5	1845.15
52657.76	100	72	28	1880.63
48896.49	100	73.5	26.5	1845.15
52657.76	100	71.5	28.5	1847.64
48896.49	100	73.5	26.5	1845.15
52657.76	100	71	29	1815.78
52657.76	100	71	29	1815.78
52657.76	100	71.5	28.5	1847.64
52657.76	100	71.5	28.5	1847.64
52657.76	100	71.5	28.5	1847.64
52657.76	100	72	28	1880.63

Appendix-4: Experimental data for rectangular shaped micro-grooved copper plate

Table 15: Experimental data for rectangular shaped micro-grooved copper plate

Time t (sec)	Upper surface temperature T ₁ (°C)	Lower surface temperature T ₃ (°C)	Cooling water inlet temperature T ₅ (°C)	Cooling water outlet temperature T ₂ (°C)	Steam inlet temperature T ₄ (°C)
30	39	59	29	33	100
60	47	63	29	36	100
90	54	65	29	38	100
120	60	66	29	39	100
150	63	66	29	40	100
180	64	68	29	40	100
210	66	69	29	40	100
240	68	69	29	41	100
270	66	70	29	41	100
300	68	71	29	42	100
330	68	70	29	41	100
360	67	71	29	42	100
390	68	71	29	42	100
420	68	71	29	43	100
450	68	71	29	43	100
480	68	71	29	43	100
510	68	72	29	43	100
540	68	71	29	43	100
570	68	71	29	44	100
600	68	71	29	44	100
630	68	72	29	43	100
660	68	71	29	44	100

690	68	72	29	44	100
720	68	72	29	44	100
750	69	72	29	44	100
780	69	72	29	44	100
810	68	73	29	44	100
840	69	73	29	44	100
870	69	73	29	44	100
900	69	74	29	44	100
930	67	76	29	44	100
960	66	76	29	44	100
990	67	76	29	44	100
1020	67	75	29	44	100
1050	67	76	29	44	100
1080	67	76	29	44	100
1110	68	76	29	44	100
1140	67	77	29	44	100
1170	67	78	29	44	100
1200	68	77	29	44	100
1230	69	77	29	44	100
1260	69	78	29	44	100
1290	69	77	29	44	100
1320	69	77	29	44	100
1350	68	78	29	44	100
1380	68	78	29	44	100
1410	70	77	29	44	100
1440	69	78	29	44	100
1470	69	78	29	44	100
1500	70	77	29	44	100
1530	69	77	29	44	100
1560	69	78	29	44	100
1590	68	78	29	44	100

1620	68	78	29	44	100
1650	69	77	29	44	100
1680	69	77	29	44	100
1710	68	78	29	44	100
1740	69	78	29	44	100
1770	70	77	29	44	100
1800	68	78	29	44	100
1830	69	78	29	44	100
1860	69	78	29	44	100
1890	70	77	29	44	100
1920	69	78	29	44	100

Table 16: Calculation of area and mass flow rate for rectangular shaped micro-grooved copper plate

Total time of water collection	Effective condensation heat transfer area	Mass of water collected	Mass flow rate of water
t (sec)	A (m ²)	m (kg)	\dot{m} (kg/sec)
180	0.016	2.588	0.01438

Table 17: Calculation of heat flux for rectangular shaped micro-grooved copper plate

Upper surface temperature T_1 (°C)	Lower surface temperature T_3 (°C)	Cooling water inlet temperature T_5 (°C)	Cooling water outlet temperature T_2 (°C)	Calculated heat flux q (W/m ²)
39	59	29	33	15045.07
47	63	29	36	26328.88
54	65	29	38	33851.41
60	66	29	39	37612.68

63	66	29	40	41373.95
64	68	29	40	41373.95
66	69	29	40	41373.95
68	69	29	41	45135.22
66	70	29	41	45135.22
68	71	29	42	48896.49
68	70	29	41	45135.22
67	71	29	42	48896.49
68	71	29	42	48896.49
68	71	29	43	52657.76
68	71	29	43	52657.76
68	71	29	43	52657.76
68	72	29	43	52657.76
68	71	29	43	52657.76
68	71	29	44	56419.03
68	71	29	44	56419.03
68	72	29	43	52657.76
68	71	29	44	56419.03
68	72	29	44	56419.03
68	72	29	44	56419.03
69	72	29	44	56419.03
69	72	29	44	56419.03
68	73	29	44	56419.03
69	73	29	44	56419.03
69	73	29	44	56419.03
69	74	29	44	56419.03
67	76	29	44	56419.03
66	76	29	44	56419.03
67	76	29	44	56419.03
67	75	29	44	56419.03
67	76	29	44	56419.03

67	76	29	44	56419.03
68	76	29	44	56419.03
67	77	29	44	56419.03
67	78	29	44	56419.03
68	77	29	44	56419.03
69	77	29	44	56419.03
69	78	29	44	56419.03
69	77	29	44	56419.03
69	77	29	44	56419.03
68	78	29	44	56419.03
68	78	29	44	56419.03
70	77	29	44	56419.03
69	78	29	44	56419.03
69	78	29	44	56419.03
70	77	29	44	56419.03
69	77	29	44	56419.03
69	78	29	44	56419.03
68	78	29	44	56419.03
68	78	29	44	56419.03
69	77	29	44	56419.03
69	77	29	44	56419.03
68	78	29	44	56419.03
69	78	29	44	56419.03
70	77	29	44	56419.03
68	78	29	44	56419.03
69	78	29	44	56419.03
69	78	29	44	56419.03
70	77	29	44	56419.03
69	78	29	44	56419.03

Table 18: Calculation of heat transfer Co-efficient for rectangular shaped micro-grooved copper plate

Calculated heat flux q (W/m ²)	Steam inlet temperature T_4 (°C)	Surface temperature of copper plate T_{surf} (°C)	Temperature difference ΔT (°C)	Heat transfer Co-efficient h_c (W/m ² .°C)
15045.07	100	49	51	295.00
26328.88	100	55	45	585.08
33851.41	100	59.5	40.5	835.83
37612.68	100	63	37	1016.55
41373.95	100	64.5	35.5	1165.46
41373.95	100	66	34	1216.88
41373.95	100	67.5	32.5	1273.04
45135.22	100	68.5	31.5	1432.86
45135.22	100	68	32	1410.47
48896.49	100	69.5	30.5	1603.16
45135.22	100	69	31	1455.97
48896.49	100	69	31	1577.30
48896.49	100	69.5	30.5	1603.16
52657.76	100	69.5	30.5	1726.48
52657.76	100	69.5	30.5	1726.48
52657.76	100	69.5	30.5	1726.48
52657.76	100	70	30	1755.25
52657.76	100	69.5	30.5	1726.48
56419.03	100	69.5	30.5	1849.80
56419.03	100	69.5	30.5	1849.80
52657.76	100	70	30	1755.25
56419.03	100	69.5	30.5	1849.80

56419.03	100	70	30	1880.63
56419.03	100	70	30	1880.63
56419.03	100	70.5	29.5	1912.50
56419.03	100	70.5	29.5	1912.50
56419.03	100	70.5	29.5	1912.50
56419.03	100	71	29	1945.48
56419.03	100	71	29	1945.48
56419.03	100	71.5	28.5	1979.61
56419.03	100	71.5	28.5	1979.61
56419.03	100	71	29	1945.48
56419.03	100	71.5	28.5	1979.61
56419.03	100	71	29	1945.48
56419.03	100	71.5	28.5	1979.61
56419.03	100	71.5	28.5	1979.61
56419.03	100	72	28	2014.96
56419.03	100	72	28	2014.96
56419.03	100	72.5	27.5	2051.60
56419.03	100	72.5	27.5	2051.60
56419.03	100	73	27	2089.59
56419.03	100	73.5	26.5	2129.02
56419.03	100	73	27	2089.59
56419.03	100	73	27	2089.59
56419.03	100	73	27	2089.59
56419.03	100	73	27	2089.59
56419.03	100	73.5	26.5	2129.02
56419.03	100	73.5	26.5	2129.02
56419.03	100	73.5	26.5	2129.02
56419.03	100	73.5	26.5	2129.02
56419.03	100	73	27	2089.59
56419.03	100	73.5	26.5	2129.02
56419.03	100	73	27	2089.59

56419.03	100	73	27	2089.59
56419.03	100	73	27	2089.59
56419.03	100	73	27	2089.59
56419.03	100	73	27	2089.59
56419.03	100	73.5	26.5	2129.02
56419.03	100	73.5	26.5	2129.02
56419.03	100	73	27	2089.59
56419.03	100	73.5	26.5	2129.02
56419.03	100	73.5	26.5	2129.02
56419.03	100	73.5	26.5	2129.02
56419.03	100	73.5	26.5	2129.02
56419.03	100	73.5	26.5	2129.02

Appendix 5: Sample calculation

Sample calculation is shown for rectangular shaped micro-grooved copper plate.

Total time of water collection, $t = 180$ s

Height of the plate, $H = 150$ mm

Width of the plate, $W = 115$ mm

Weight of empty bucket = 208gm

Weight of bucket with water = 2796 gm

Inlet temperature of cooling water $T_5 = 29^\circ\text{C}$

Specific heat of water, $c_p = 4186 \frac{\text{J}}{\text{kg} \cdot \text{K}}$

Upper surface temperature, $T_1 = 39^\circ\text{C}$

Cooling water outlet temperature, $T_2 = 33^\circ\text{C}$

Lower surface temperature, $T_3 = 59^\circ\text{C}$

Steam inlet temperature, $T_4 = 103^\circ\text{C}$

Effective Condensation heat transfer area, $A = 0.016 \text{ m}^2$

Mass flow rate of Water $\dot{m} = \frac{m}{t} = \frac{2796 - 208}{180} = 14.38 \text{ gm/sec}$

Heat Flux, $q = \dot{m}c_p(T_2 - T_5) = 15045.075 \frac{\text{W}}{\text{m}^2}$

$T_{\text{surf}} = \frac{T_1 + T_3}{2} = \frac{39 + 59}{2} = 49^\circ\text{C}$

$\Delta T = T_4 - T_{\text{surf}} = (100 - 49)^\circ\text{C} = 51^\circ\text{C}$

Heat transfer coefficient $h_c = \frac{q}{\Delta T} = 295.001 \frac{\text{W}}{\text{m}^2 \cdot \text{K}}$

Appendix 6: Sample calculation of uncertainty analysis

A sample calculation of uncertainty analysis has been shown below.

At $t = 300\text{s}$, $T_1 = 64^\circ\text{C}$, $T_2 = 36^\circ\text{C}$, $T_3 = 62^\circ\text{C}$, $T_4 = 100^\circ\text{C}$, $T_5 = 25^\circ\text{C}$.

Here, $\dot{m} = \frac{2.588}{180} = 0.0144 \frac{\text{kg}}{\text{sec}}$, $C_p = 4186 \frac{\text{J}}{\text{kg} \cdot \text{K}}$, $H = 0.15\text{m}$, $W = 0.11\text{m}$.

Now, from equation 4.7,

$$q = \frac{mc_p(T_2 - T_5)}{H \times W \times t} = \frac{2.588 \times 4186 \times (36 - 25)}{0.15 \times 0.11 \times 180} = 40123.6 \frac{\text{W}}{\text{m}^2}$$

$$\therefore \frac{\partial q}{\partial m} = \frac{c_p(T_2 - T_5)}{H \times W \times t} = \frac{4186 \times (36 - 25)}{0.15 \times 0.11 \times 300} = 9302.2$$

$$\frac{\partial q}{\partial T_5} = -\frac{mc_p}{H \times W \times t} = -\frac{2.588 \times 4186}{0.15 \times 0.11 \times 300} = -2188.6$$

$$\frac{\partial q}{\partial T_2} = \frac{mc_p}{H \times W \times t} = \frac{2.588 \times 4186}{0.15 \times 0.11 \times 300} = 2188.6$$

$$\frac{\partial q}{\partial H} = -\frac{mc_p(T_2 - T_5)}{H^2 \times W \times t} = -\frac{2.588 \times 4186 \times (36 - 25)}{0.15^2 \times 0.11 \times 300} = -16494.3$$

$$\frac{\partial q}{\partial W} = -\frac{mc_p(T_2 - T_5)}{W^2 \times H \times t} = -\frac{2.588 \times 4186 \times (36 - 25)}{0.11^2 \times 0.15 \times 300} = -218855.9$$

$$\frac{\partial q}{\partial t} = -\frac{mc_p(T_2 - T_5)}{t^2 \times W \times H} = -\frac{2.588 \times 4186 \times (36 - 25)}{300^2 \times 0.11 \times 0.15} = -80.2$$

Now, $w_m = \sqrt{0.0005^2 + 0^2} = 0.0005 \text{ kg}$, $w_{T_5} = \sqrt{0.5^2 + 0^2} = 0.5^\circ\text{C}$

$w_{T_2} = \sqrt{0.5^2 + 0.36^2} = 0.616^\circ\text{C}$, $w_H = w_W = 0.005\text{mm}$, $w_t = 0.05\text{s}$

$$\therefore w_q = \left[\left(\frac{\partial q}{\partial m} w_m \right)^2 + \left(\frac{\partial q}{\partial T_5} w_{T_5} \right)^2 + \left(\frac{\partial q}{\partial T_2} w_{T_2} \right)^2 + \left(\frac{\partial q}{\partial H} w_H \right)^2 + \left(\frac{\partial q}{\partial W} w_W \right)^2 + \left(\frac{\partial q}{\partial t} w_t \right)^2 \right]^{1/2}$$

$$= \sqrt{(9302 \times 0.0005)^2 + (-2188 \times 0.5)^2 + (2188 \times 0.616)^2 + (-16494 \times 0.000005)^2 + (-218855 \times 0.000005)^2 + (-80.2 \times 0.05)^2}$$

$$= 1348$$

\therefore Percentage of uncertainty in heat flux = $\frac{1348}{40123.6} \times 100\% = 3.4\%$

$$\text{Now, } h_c = \frac{q}{\Delta T} = \frac{40123.6}{37} = 1084.4 \frac{\text{W}}{\text{m}^2 \cdot \text{K}}$$

$$\frac{\partial h_c}{\partial q} = \frac{2}{2T_4 - T_1 - T_3} = \frac{2}{2 \times 100 - 64 - 62} = 0.027$$

$$\frac{\partial h_c}{\partial T_1} = \frac{-2q}{(2T_4 - T_1 - T_3)^2} = \frac{-2 \times 40123.6}{(2 \times 100 - 64 - 62)^2} = -14.65$$

$$\frac{\partial h_c}{\partial T_3} = \frac{2q}{(2T_4 - T_1 - T_3)^2} = \frac{2 \times 40123.6}{(2 \times 100 - 64 - 62)^2} = 14.65$$

$$\frac{\partial h_c}{\partial T_4} = \frac{-4q}{(2T_4 - T_1 - T_3)^2} = \frac{-4 \times 40123.6}{(2 \times 100 - 64 - 62)^2} = -29.3$$

$$w_{T_1} = \sqrt{0.5^2 + 0.772^2} = 0.92^\circ\text{C}, w_{T_3} = \sqrt{0.5^2 + 0.36^2} = 0.616^\circ\text{C}, w_{T_4} = 0.5^\circ\text{C}$$

$$\begin{aligned} \therefore w_{h_c} &= \left[\left(\frac{\partial h_c}{\partial q} w_q \right)^2 + \left(\frac{\partial h_c}{\partial T_1} w_{T_1} \right)^2 + \left(\frac{\partial h_c}{\partial T_3} w_{T_3} \right)^2 + \left(\frac{\partial h_c}{\partial T_4} w_{T_4} \right)^2 \right]^{\frac{1}{2}} \\ &= \sqrt{(0.027 \times 1348)^2 + (-14.65 \times 0.92)^2 + (14.65 \times 0.616)^2 + (-29.3 \times 0.5)^2} \\ &= 43.62 \end{aligned}$$

$$\therefore \text{Percentage of uncertainty in heat transfer coefficient} = \frac{43.62}{1084.4} \times 100\% = 4\%$$